M 2020

U.PORTO
FEUP FACULDADE DE ENGENHARIA
UNIVERSIDADE DO PORTO

THE POTENTIAL OF ASPEN ADSORPTION™ SOFTWARE PACKAGE TO SIMULATE PRESSURE SWING ADSORPTION UNITS

ANA GABRIELA ALVES VERDADE

DISSERTAÇÃO DE MESTRADO APRESENTADA
À FACULDADE DE ENGENHARIA DA UNIVERSIDADE DO PORTO EM
ENGENHARIA QUÍMICA

Master in Chemical Engineering

The potential of Aspen Adsorption™ software package to simulate pressure swing adsorption units

Master dissertation

of

Ana Gabriela Alves Verdade

Developed within the course of Dissertation

held in

CoLAB Net4CO$_2$ - NETwork for a Sustainable CO$_2$ Economy



Supervisor at FEUP: **Prof. Fernando G. Martins**

Supervisor at Net4CO2: **Dr. Mariana G. Domingos**

U.PORTO
FEUP FACULDADE DE ENGENHARIA
UNIVERSIDADE DO PORTO

DEPARTAMENTO DE
ENGENHARIA QUÍMICA

July 2020

Acknowledgement

Developing a Master dissertation during such a particular period in the world's history as the one we are living right now, was not ideal. However, times like these make us truly reflect upon what's important in our lives and in my case, made me thankful for all the support I realized I had.

To my supervisors, Professor Fernando Martins and Dr. Mariana Domingos, for all the precious advice and guidance, for compelling me to work harder every day and for the constant availability and support throughout this period.

To the Faculty of Engineering of University of Porto and all my professors, for pushing me to my limits during the last five years, making me grow as a person and capable professional, turning me into the engineer I've just become. Also, to Net4CO2, for providing all the necessary means for the realization of this dissertation and for the confidence placed in my work.

To all my family, for the unconditional support that never ceased. To my parents for offering me all the tools that allowed me to be here today, to my brother and sister for making sure I have a reason to laugh every day and to my grandmother for always being so present and encouraging.

To Pedro, my first reader, for being with me in every step of the way, for motivating me more than anyone else, for all the patience and for giving me confidence to pursue all my goals.

Finally, to all my friends, for the great moments we lived. To the ones I met at FEUP, for sharing and calming all my worries and for all the fun we had. To the ones from before, for all the memories we built and for supporting me for so many years.

This work was financially supported by: Base Funding - UIDB/50020/2020 of the Associate Laboratory LSRE-LCM - funded by national funds through FCT/MCTES (PIDDAC).

Professor Fernando Martins, supervisor of this dissertation is an integrated member of LEPABE – Laboratory for Process Engineering, Environment, Biotechnology and Energy, financially supported by: Base Funding - UIDB/00511/2020 of the Laboratory for Process Engineering, Environment, Biotechnology and Energy – LEPABE - funded by national funds through the FCT/MCTES (PIDDAC).





Abstract

This thesis explores the capabilities of Aspen Adsorption to simulate Pressure Swing Adsorption units (PSA). These units are frequently used for carbon dioxide and hydrogen separations in scenarios involving the production of synthetic fuels and hydrogen. Such scenarios are of extreme relevance to the carbon dioxide circular economy, which is the main focus of the Net4CO2 Collaborative Laboratory.

A literature review was performed to understand the software's acceptance and its main applications, followed by a hands-on exploration of the software and its main features. A flow diagram was then constructed to summarize the main steps in every Aspen Adsorption simulation, and a deeper analysis of its necessary inputs, governing equations, available numerical methods and possible outputs was conducted.

The first case analyzed in detail was the adsorption and desorption phenomena in a single column and the response to different valve settings. Then, a comparative study of two simulation flowsheet models for PSA simulations was performed, and the comparison between the two simulation modes available in the software for gas cyclic separations was established. Aspen Adsorption was then used to reproduce previously published results for hydrogen separations using PSA units. A breakthrough curve was reproduced, and a PSA unit's performance compared, considering the purity and recovery obtained as well as the predicted axial profiles. Finally, a simulation of a PSA unit for H_2 separation at a larger scale was performed using this software.

It was concluded that Aspen Adsorption is a complete and powerful tool for the simulation and optimization of adsorption processes, including PSA units. The flowsheet model which solves the governing equations for each element of the system seems to be easier to understand and control than that which replaces similar elements of the system by fictional units (where the information is just stored and replayed at different steps of the cycle). Regarding the different simulation modes available, the gCSS led to results closer to the published ones in the hydrogen separations considered, but a more in-depth study is suggested to fully understand the differences observed in the two modes. The use of this software also presents some challenges to the general user regarding the acceptance and prediction of non-realistic conditions without retrieving error or warning messages (e.g. compositions for streams with null flow and reverse flow in some valves).

Keywords: Pressure Swing Adsorption (PSA), Adsorption processes, Aspen Adsorption, Simulation

Resumo

Esta tese explora a capacidade do Aspen Adsorption para simular unidades de Adsorção com Modulação de Pressão (do inglês, PSA). Estas unidades são frequentemente usadas para separações de hidrogénio e dióxido de carbono em cenários que envolvem a produção de combustíveis sintéticos e hidrogénio. Tais cenários são de extrema importância para a economia circular de dióxido de carbono, que é o maior foco do laboratório colaborativo Net4CO2.

Foi realizada uma revisão bibliográfica para compreender a aceitação do programa e as suas principais aplicações, seguida de uma exploração prática do mesmo para entender como funciona e quais são as suas principais funcionalidades. Foi também construído um diagrama de fluxo que resume os principais passos em qualquer simulação no programa e conduzida uma análise das suas entradas, das equações governativas, dos métodos numéricos disponíveis e possíveis saídas.

O primeiro caso analisado em detalhe foi o fenómeno de adsorção e dessorção numa coluna e a sua resposta a diferentes configurações de válvulas. Seguidamente, foi efetuado um estudo comparativo dos dois modelos de diagramas de simulação para unidades de PSA, bem como a comparação entre os dois modos de simulação para separações gasosas cíclicas. O Aspen Adsorption foi, então, utilizado para reproduzir resultados publicados para separações de hidrogénio em unidades de PSA. Foi replicada uma curva de rutura e o desempenho de uma unidade de PSA foi comparada, considerando a pureza e recuperação obtidas, bem como os perfis axiais. Por fim, efetuou-se uma simulação de uma unidade de PSA para separação de H_2 a uma escala superior.

Conclui-se que o Aspen Adsorption é uma ferramenta completa e poderosa para a simulação e otimização de processos de adsorção, incluindo unidades de PSA. O diagrama de simulação que resolve as equações governativas para cada elemento do sistema parece ser mais simples de entender e controlar do que aquele que substitui elementos reais por unidades fictícias (onde a informação é apenas guardada e reproduzida noutro passo do ciclo). Quanto aos modos de simulação, o modo gCSS fornece resultados próximos dos publicados nas separações consideradas, mas é sugerido um estudo mais aprofundado para entender as diferenças observadas entre os dois modos de simulação. O uso deste programa apresenta alguns desafios ao utilizador relacionados com a previsão de condições não realistas, sem apresentar mensagens de erro ou aviso (ex: composições de correntes com caudal nulo e fluxo reverso em válvulas).

Palavras-chave: Adsorção com Modulação de Pressão (PSA), Processos de adsorção, Aspen Adsorption, Simulação

Declaration

I hereby declare, under word of honor, that this work is original and that all non-original contributions are indicated, and due reference is given to the author and source.

Sign and date,

Ana Vandade

July 6th, 2020

Index

1 Introduction 1

1.1 Framework and project presentation 1

1.2 Project contribution 2

1.3 Thesis' structure 2

2 State of the art 4

2.1 The need for hydrogen and alternative fuels 4

2.2 Adsorption and Pressure Swing Adsorption (PSA) 5

2.3 Literature review using PRISMA Methodology 7

2.4 Aspen Adsorption 8

3 Aspen Adsorption, an overview 9

3.1 Adding the components 9

3.2 Choosing between Dynamic or gCSS simulation modes 10

3.3 Building the flowsheet and defining the blocks' specifications 10

3.4 Specifications of the adsorption bed 12

3.4.1 The geometry window 12

3.4.2 The adsorbent properties window 12

3.4.3 Material and momentum balances window 12

3.4.4 Kinetics (Resistances to mass transfer) window 13

3.4.5 Equilibrium (Isotherm) window 14

3.4.6 Energy Balance window 15

3.4.7 Reaction window 17

3.5 Adding the cycle organizer 17

3.6 Choosing the numerical methods and solver options 18

3.7 Initializing, running and extracting the results 20

4 Simulation of a PSA unit using Aspen Adsorption 21

4.1 The case study 21

4.2. Two-step cycle on a single bed 22

4.2.1 Analysis of cycle 1 23
4.2.2 Analysis of cycle 2 24
4.3. Two models for PSA simulations 27
4.4. Two simulation modes 33
5 Validation of Aspen Adsorption's results 35
5.1 Analysis of a breakthrough curve 35
5.2 Analysis of a PSA unit for H_2 separation 37
5.2.1 Flowrate control 38
5.2.2 Purity and Recovery 40
5.2.3 Axial profiles 42
5.3 Simulation of a PSA Unit for H_2 Separation at Industrial Scale 43
6 Conclusions 47
6.1 Accomplished objectives 48
6.2 Limitations and Future Work 48
6.3 Final assessment 48
7 References 49
Appendices 51
Appendix A – PRISMA Methodology 51
Appendix B – Numerical methods 52
Appendix C – Isotherm adjustments (gCCS to Dynamic) 53
Appendix D – Bed Specifications for cases simulated in Chapter 5 55
Appendix E – Attempts to use a constant feed flowrate during a PSA experiment 56
Appendix F – Derivation of the CV expression for pressurization and depressurization valves 57

List of Figures

Figure 1 - Representation of a typical PSA cycle [8]. 6

Figure 2 – Flow diagram for the main steps for a simulation in Aspen Adsorption. 9

Figure 3 – Main Aspen Adsorption's models with Gas Dynamic terminology. 12

Figure 4 - The cycle organizer. 17

Figure 5 - Visual representation of the Method of Lines [13]. 18

Figure 6 - Visual representation of the discretization method available in gCSS mode [13]. 19

Figure 7 - Example of a 2D and a 3D plot from Aspen Adsorption. 20

Figure 8 - Process flowsheet of the two-step cycle simulation on a single bed. 22

Figure 9 - Variation of the Product (P1) flowrate. 24

Figure 10 - Variation of O_2 and N_2 molar fractions in the product stream (P1). 25

Figure 11 - Variation of the Waste (W1) flowrate during the desorption step. 25

Figure 12 - Breakthrough curve. 26

Figure 13 - Simulation flowsheet for Model 1. 27

Figure 14 - Simulation flowsheet for Model 2. 28

Figure 15 - N_2 molar fraction in P1 for Model 1 and 2 during 15 cycles. 29

Figure 16 - N_2 molar fraction in P1 for Model 1 and 2 during the first 2 cycles. 30

Figure 17 - N_2 molar fraction in TD2, TOP1, TOP2 and TP during the first 4 cycles. 31

Figure 18 - Effect of TP's volume on the product's N2 molar composition. 32

Figure 19 - Simulation flowsheets of a Dynamic and gCSS simulation. 33

Figure 20 - N_2 molar fraction in P1 in a Dynamic and gCSS simulation. 34

Figure 21 - Breakthrough curve obtained in Aspen Adsorption and in Jee et al. 36

Figure 22 - Molar fractions of the components in the product stream, during 10 cycles. 40

Figure 23 - Pressure inside Bed 1 during 10 cycles. 40

Figure 24 - Comparison of the molar fractions of components in the product stream for in the gCSS and Dynamic simulation, during 10 cycles. 41

Figure 25 - H_2 molar fraction along the bed length at the end of the adsorption step of cycle 10. 42

Figure 26 - CH_4 solid loading along the bed length at the end of the adsorption step of cycle 10. 43

Figure 27 - Molar fractions of the components in the product stream for the industrial and lab scale cases during 10 cycles. 45

Figure 28 - Pressure variation in Bed 1 along the 10 cycles for industrial and lab scale cases during 10 cycles. 45

Figure 29 - Pressure variation in Bed 1 in the first 100 seconds of the simulation, with a feed flowrate unable to fully pressurize the bed. 46

List of Tables

Table 1 - Set of units considered by Aspen Adsorption in isotherm parameters 15

Table 2 - Isotherm parameters for each component 21

Table 3 - Specifications of the case study 22

Table 4 - Summary of two-step cycle's configurations 23

Table 5 - Specifications of the cycle for Model 1 28

Table 6 - Specifications of the cycle for Model 2 29

Table 7 - Specification of the PSA cycle for the H_2 separation 39

Table 8 - Purity and recovery values from Aspen Adsorption simulations compared with the values in Yang et al. 42

Table 9 - Parameters calculated for the lab scale and industrial scale cases 44

Notation and Glossary

A_{Hi}	Internal wall element area for heat transfer	m
A_{Ho}	External wall element area for heat transfer	m
a_p	Particle external surface area to particle volume ratio	m^{-1}
C_i	Gas phase concentration for component i	kmol m^{-3}
C_i^*	Equilibrium gas phase concentration for component i	kmol m^{-3}
C_{Ps}	Solid heat capacity	MJ kg^{-1} K^{-1}
C_{Pw}	Wall material heat capacity	MJ kg^{-1} K^{-1}
CV	Valve's coefficient	kmol s^{-1} bar^{-1}
C_{vg}	Gas mixture heat capacity	MJ kg^{-1} K^{-1}
d_{bi}	Internal bed diameter	m
D_{Li}	Axial dispersion coefficient for component i	m^2 s^{-1}
d_p	Particle diameter	m
F_m	Molar flowrate of stream m	$kmol_T$ s^{-1}
H_{amb}	Wall/Environment heat transfer coefficient	MW m^{-2} K^{-1}
H_b	Bed height	m
H_s	Fluid/Solid heat transfer coefficient	MW m^{-2} K^{-1}
H_w	Fluid/Wall heat transfer coefficient	MW m^{-2} K^{-1}
IP_{xi}	Isotherm parameter x for component i	-
k_{Fi}	Fluid mass transfer coefficient for component i	s^{-1}
k_g	Gas mixture thermal conductivity	MW m^{-1} K^{-1}
k_{Si}	Solid mass transfer coefficient for component i	s^{-1}
k_s	Solid phase thermal conductivity	MW m^{-1} K^{-1}
k_w	Wall thermal conductivity	MW m^{-1} K^{-1}
m_{ads}	Mass of adsorbent/solid	kg
M_w	Molecular weight of gaseous mixture	kg $kmol^{-1}$
P	Pressure	bar
$P_{B\ start}$	Bed pressure at the start of the step	bar
$P_{B\ end}$	Bed pressure at the end of the step	bar
$P_{Ext\ start}$	External pressure at the start of the step	bar
$P_{Ext\ end}$	External pressure at the end of the step	bar
Pe	Peclet number	-
Q_i	Amount adsorbed or Solid loading for component i	kmol kg_{ads}^{-1}
Q_i^*	Equilibrium amount adsorbed or Solid loading for component i	kmol kg_{ads}^{-1}
R	Ideal gas constant	L atm K^{-1} mol^{-1}
r_p	Particle radius	m
t	Time	s
T_{amb}	Environment temperature	K
T_B	Temperature of the bed	K
T_g	Gas temperature	K
T_s	Solid temperature	K
t_{step}	Step duration	s
T_w	Wall temperature	K
V_B	Volume of the bed	m^3
V_{bulk}	Volume of the bulk	m^3
v_g	Superficial gas velocity	m s^{-1}
V_{Hi}	Internal wall element volume for heat transfer	m^2
V_{Ho}	External wall element volume for heat transfer	m^2
V_{TP}	Volume of the tank TP	m^3
x	Axial distance coordinate	m
y_{im}	Molar fraction of component *i* on stream m	$kmol_i$ $kmol_T^{-1}$
w_t	Wall thickness	m

Greek Letters

ε_b	Interparticle or bed porosity	-
ε_t	Total porosity	-
ε_p	Intraparticle porosity	-
ΔH_i	Enthalpy of adsorption for component i	MJ kmol^{-1}
ΔP	Pressure drop through the valve	bar
ρ_b	Bed packing density	kg m^{-3}
ρ_g	Gas density	kmol m^{-3}
ρ_p	Particle or solid density	kg m^{-3}
ρ_w	Wall material density	kg m^{-3}
μ_g	Gas mixture viscosity	cP
Ψ	Particle shape factor	-

List of Acronyms

CMS	Carbon Molecular Sieve
CSS	Cyclic Steady State
CV	Valve coefficient
gCSS	gas Cyclic Steady State
IAS	Ideal Adsorbed Solution
ISA	International Society of Automation
LDF	Linear Driving Force approximation
LRC3	Loading Ratio Correlation 3
ODE	Ordinary differential equations
PDE	Partial differential equations
PSA	Pressure Swing Adsorption
PRISMA	Preferred Reporting Items for Systematic Reviews and Meta-Analyses
QDF	Quadratic Driving Force approximation
R&D	Research and Development
SMR	Steam Methane Reforming
TSA	Temperature Swing Adsorption
VSA	Vacuum Pressure Swing Adsorption

1 Introduction

1.1 Framework and project presentation

Most of the world's energy production is highly dependent on fossil fuels, which raises two major concerns: i) they are non-renewable sources and are limited by the available resources; ii) the energy is obtained from its combustion, implying the release of a substantial amount of particles as well as the increase of the concentrations of CO_2 in the atmosphere. The environmental threat of these calls for an international action, for promoting a change in the energy system worldwide, which can reduce the dependence on fossil fuels and reduce or even reverse the environmental impacts caused by their utilization.

The collaborative laboratory Net4CO2 aims to make a substantial contribution to this action and for that purpose, technical solutions are developed on two main fronts: i) an efficient and profitable way of capturing/separating CO_2 and, ii) a competitive production of alternative fuels such as synthetic fuels and hydrogen. The potential of the proposed technical solutions from economic and environmental perspectives is evaluated through several stages during their development, recurring to process simulation tools to simulate the overall process, where the solution will be integrated, and its performance analyzed on a larger scale.

Aspen Tech ® simulation packages, such as Aspen Plus, Aspen Energy Analyzer, Aspen Exchanger Design and Rating and Aspen Process Economic Analyzer are the software packages already used at Net4CO2. Aspen Plus is the main software tool used for the mass and energy balances, and for the required design and thermodynamic calculations for a given process flow diagram with different process units. This software tool is not prepared for simulating dynamic specific processes, such as Pressure Swing Adsorption (PSA) units. For such processes, Aspen Tech ® has a package called Aspen Adsorption, whose results may be exported to Aspen Plus.

This software package is currently at the early stages of utilization at Net4CO2 and the main objective of this thesis is to go further in the exploration of Aspen Adsorption software capability to simulate PSA processes, as well as understanding the advantages and disadvantages of its use. These units typically occur in scenarios involving hydrogen or synthetic fuels production by Steam Methane Reforming or in scenarios involving the adjustment of the H_2/CO ratio for the Fisher-Tropsch process.

To arrive to the final objective, a literature review has been performed to understand the software's acceptance and its main applications, followed by the execution of some tutorials to a hands-on exploration of the software and its main features. After the execution of the different tutorials, a comparative study on how to simulate Pressure Swing Adsorption

units using Aspen Adsorption was executed. Finally, some published cases for H_2 separation by a PSA process were compared with Aspen Adsorption's results, a strategy was developed for the flowrate control and a simulation of a PSA unit at a larger scale was performed using this software.

1.2 Project contribution

The simulation of adsorption processes using Aspen Adsorption software package is, on itself, a relevant effort not only from Net4CO2's perspective but also for the Faculty of Engineering of University of Porto, since as far as it is known, it is the first time the use of this software will be formally attempted in the scope of a Master thesis.

Efforts were made to understand how Aspen Adsorption works from its governing equations to its numerical methods. In addition, the goal of this work is to have a better grasp on the main advantages and disadvantages of this software and in understanding the finest way to simulate PSA units, by choosing the suitable numerical methods, simulation modes and other tools available by the software package. Some published papers were also simulated using Aspen Adsorption software tool in order to critically analyze the software's results.

1.3 Thesis' structure

The present dissertation is divided into six chapters. Chapter 1 describes the framework, the project presentation and its relevance, as well as its main objectives.

The second chapter is the State of the Art. Section 2.1 contextualizes the importance of developing alternatives for fossil fuels and presents hydrogen as a pertinent solution. In Section 2.2, adsorption and particularly Pressure Swing Adsorption's principles are analyzed. A literature review using PRISMA Methodology is presented in Section 2.3 in order to understand the acceptance of Aspen Adsorption software package and its main applications. Finally, in Section 2.4, this software is introduced as a useful simulation tool.

In Chapter 3, an overview of Aspen Adsorption is presented, where the main features of the software are summarized, from its necessary inputs to its possible outputs, acknowledging the main equations that rule adsorption processes and how they are solved using the available numerical methods.

The fourth chapter delves into the studies performed for Pressure Swing Adsorption simulations using Aspen Adsorption software package. Section 4.1 presents the case study used for this analysis; Section 4.2 presents the study of the simulation of a two-step cycle on a single bed in order to understand the adsorption and desorption phenomena in detail; Section 4.3 compares two simulation flowsheets for PSA simulations in Aspen Adsorption: Model 1 and Model

2; finally, Section 4.4 compares the two simulation modes available in the software: gCSS and Dynamic mode.

Chapter 5 delves into the validation of Aspen Adsorption's results. In Section 5.1 a study of the breakthrough curve for the $H_2/CH_4/CO$ system is performed and compared with the results of Jee et al. [16]; Section 5.2 presents the study of a PSA unit for H_2 separation from a H_2/CH_4 mixture, including the comparison of the purity, recovery and axial profiles of the simulations performed with the experimental and predicted values in the work of Yang et al. [17]; Section 5.3 presents the simulation of an H_2 separation by PSA at an industrial scale using Aspen Adsorption.

Finally, the sixth chapter presents the main conclusions of this work, including some reflections on the limitations and the suggested future work.

2 State of the art

2.1 The need for hydrogen and alternative fuels

Carbon dioxide, methane and other greenhouse gases are one of the major causes of the environmental changes that the planet has faced in the latest years. In fact, the Earth's average surface temperature has risen about 0.9 ºC since the late 19th century, a change driven mainly by human-made emissions into the atmosphere. Most of the warming occurred in the past 35 years, with the five warmest years on record taking place since 2010 [1].

Energy production, especially from fossil fuels such as oil, natural gas and coal, is one of the largest sources of global greenhouse-gas emissions, being transportation sector its major contributor, causing 32% of CO_2 emissions in the European Union [2]. In order to meet the world's agreed climate target defined under the Paris Agreement in 2015, energy-related carbon dioxide emissions should be limited to 770 megatons per year by 2050 [3].

Due to these environmental concerns, alternatives to fossil fuels have been explored, but in order to be significant, those alternatives must be technically feasible, economically competitive, environmentally satisfactory and willingly accessible. Hydrogen has increasingly received attention since it is a promising environmentally friendly and versatile energy carrier [4], which can be used in fuel cells and might potentially enable a full largescale integration of renewables, in response to the decarbonization and the growing hesitations surrounding fossil fuels [3].

The amount of energy produced per unit mass during hydrogen combustion is higher than the one generated by other fuels such as methane, gasoline or coal [5] and it does not involve emissions such as volatile organic compounds, nitrogen oxides, sulfur oxides and particles. Therefore, the demand of hydrogen is continuously increasing with the resulting worldwide attention and research motivation for advances in the field of hydrogen production [6].

Hydrogen is an abundant element on the Earth, but rarely in the form of a gaseous compound of H_2. Typically, catalytic reforming of natural gas, such as steam methane reforming (SMR), combined with a water gas shift reaction step is used for hydrogen production at a commercial scale since it is the most cost-effective process. Nevertheless, SMR originates an H_2 stream (60-90 in molar percentage), containing several impurities for instance water vapor, CH_4, CO_2, N_2 and CO [6].

Currently, several techniques are used for hydrogen separation for achieving the target purity to be used in several processes. The use of hydrogen in fuel cells applications, for

instance, requires H_2 with a purity higher than 99.9%, and in order to reach these target values, Pressure Swing Adsorption (PSA) or Catalytic Purification are the best candidates [4].

PSA is more commonly used since it has several attractive characteristics such as low energy requirements, low capital investment costs [3] to produce hydrogen with purity up to 99.999% and recovery values between 70% and 90%, plus being operative in most physical, biological and chemical systems [7]. Industrial PSA units typically include a set of columns packed with an adsorbent, which operates simultaneously in an adsorption/regeneration cycle [3]. Nonetheless, before analyzing the details of a PSA unit, some notions on the adsorption process should be considered.

2.2 Adsorption and Pressure Swing Adsorption (PSA)

Gas separations via a selective affinity to a solid phase are considered relevant industrial challenges, however, most gas-adsorptive separations known today were already patented in the 1950s. Thus, it is fair to say that adsorption technologies are well understood and there are many resources available for its study [8].

Adsorption is the name given to the spontaneous phenomenon of attraction that a molecule from a bulk fluid phase experiences when it is close to the surface of a solid, named adsorbent [11]. Unlike absorption, which involves the entire absorbent volume, adsorption is a function of the active surface area, so the adsorbents are usually porous materials that can selectively adsorb and desorb gases, regenerating the adsorbent, depending on the operating conditions. There are only a limited number of methods that can accomplish the desorption or release in the regenerating phase and these methods characterize the gas adsorption technologies. When regeneration is accomplished by changing the pressure, the process is called Pressure Swing Adsorption (PSA). In the case of accomplishment by temperature change, the process is named Temperature Swing Adsorption (TSA) and if the PSA process involves vacuum, it is referred to as Vacuum Pressure Swing Adsorption (VPSA or VSA) [8].

Adsorption involves the diffusion of a component from the bulk fluid into the pores of a solid particle and the binding of that component to the solid surface inside the pores. The driving force for the migration of the chemical species into the pore phase is the concentration difference. Hence, if the pore phase is poor in a component that the bulk phase is rich in, that component will be driven to diffuse into the pores.

The feed stream, containing the mixture of gases, contacts with the adsorbent, which is usually packed in fixed beds. The light component breaks through the column faster than the rest of the components in the mixture and, in order to accomplish separation, the feed should be stopped before any other heavy component breaks through. In addition, the adsorbent must be regenerated by desorbing all the heavy compounds, which can be done by changing the

process parameters, as mentioned before. Consequently, it is essential to have a sequential valve arrangement that allows the feed to be stopped and the total pressure of the column to be reduced at the same time, when the adsorbent is saturated [10].

Pressure Swing Adsorption (PSA) is a technology used to separate some gas species from a mixture of gases under pressure according to the species' molecular characteristics and affinity for an adsorbent material. PSA is a fully developed and commercialized technology for gas separation [9], and because it is extremely versatile, it can have a wide range of applications such as solvent vapor recovery, gas drying, air fractionation, and hydrogen production [10].

A PSA unit requires two main zones between which the total pressure of the system "swings": a high-pressure zone to facilitate adsorption and a low-pressure zone to facilitate desorption, regenerating the adsorbent. In order to operate the PSA unit cyclically, each column experiences a series of events like opening and closing valves or changing the flowrate direction. The sum of all these steps is named a cycle, and after some repetitions, the cyclic steady state (CSS) is reached and the performance of the PSA is approximately constant over time [11]. The typical PSA unit has at least two columns that follow the "Skarstrom cycle" and its four steps: pressurization, adsorption, blowdown (or depressurization) and purge [8]. The first column is always two steps ahead of the second one and it is possible to add supplementary pressure equilibration steps that enable energy savings, resulting in 6 steps in total. Figure 1 represents a schematic view of those steps.

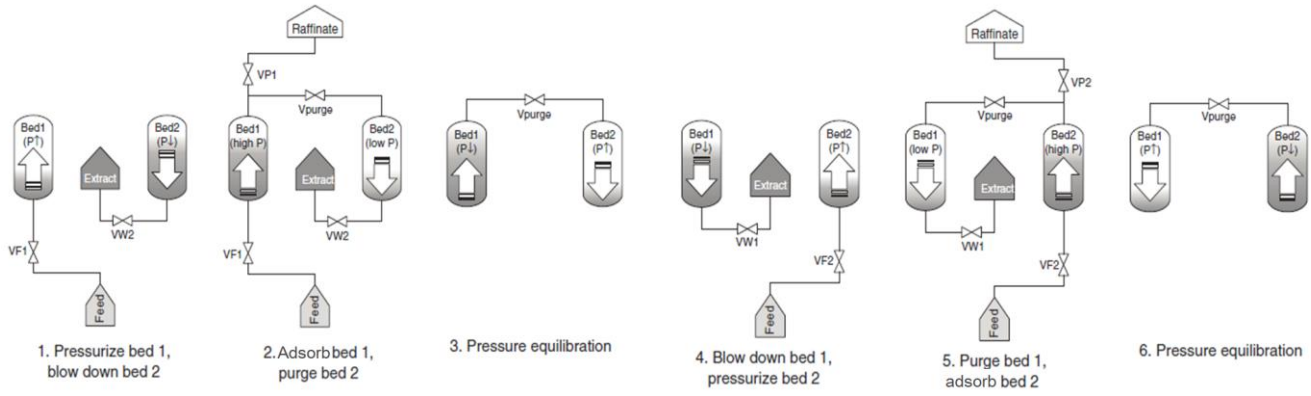


Figure 1 - Representation of a typical PSA cycle [8].

In the first step of the cycle, the feed stream (containing component W and component P) flows into bed 1 and raises its pressure while the fully loaded bed 2 is connected to the extract product reservoir, typically at atmospheric pressure, decreasing the bed pressure during this process. This step ends when the desired pressure is reached in both beds. In the second step, bed 1 strongly adsorbs the component W while component P is being stored as raffinate and some of it is being sent to bed 2 through the purge valve. This step ends when

bed 1 is fully saturated and bed 2 is fully regenerated, in other words, when the adsorbed component W has been released back into the fluid phase in bed 2. In the optional third step, the high-pressure bed 1 is connected to the low-pressure bed 2, causing a pressure equilibrium between both. Finally, in the last three steps, the cycle repeats itself, switching the beds: bed 1 is in the blowdown step while bed 2 is the pressurization step, after that, bed 1 goes through the purge phase while in bed 2 the adsorption phase occurs, and finally another pressure equilibration step might occur [8].

It is important to notice that although the columns operate on a discontinuous mode, the feed stream is continuously being used if both columns are synchronized [11]. The performance of the PSA unit is mostly determined by the adsorbent that is being used, however, engineering efforts can be placed in strategize an effective way to regenerate the adsorbent for improving performance as far as possible.

2.3 Literature review using PRISMA Methodology

There are some software packages capable of simulating an adsorption process or a Pressure Swing Adsorption unit. In this dissertation, Aspen Adsorption software package and its potentialities will be explored, studied and scrutinized.

An extensive literature review, on which PRISMA Methodology [15] was applied, was made in order to obtain a systematic review of the main R&D applications for Aspen Adsorption software package, particularly for H_2 separation in a PSA unit. The main rationale of the review was to acquire knowledge on how to use Aspen Adsorption in order to simulate real scenarios and to understand the usefulness of this software package, especially in PSA separations.

The present review includes papers and studies published from 2001 to January 2020 in the following databases: Google Scholar, Science Direct, AIChe Journal, I&EC Research and Scopus. There were no language restrictions nonetheless all the relevant publications found were in English as the keywords used were “Aspen Adsorption”, “Aspen Adsorption PSA”, “Aspen Adsorption H_2”, “H_2 separation simulation” and H_2 PSA simulation”.

A total of 57 publications were found with potential interest from the initial search and were screened based on the context of their research. The ones that didn’t include process simulations were immediately eliminated. From those, 54 publications remained, and their abstracts were appropriately reviewed. At this point, exclusions were based on the following eligibility criteria: i) the ones that didn’t describe the separation of H_2 were excluded, ii) the ones that didn’t refer to PSA or other cyclic processes for H_2 separation were left out, iii) the ones that didn’t run simulations in Aspen Adsorption and/or didn’t compare the simulations’ results with experimental data were deleted.

In the end, a total of 8 publications were reviewed in detail. The flow diagram, in Appendix A, is a visual representation of the screening process, exhibiting the number of studies identified and included/excluded.

From the 8 reviewed publications, 2 papers were chosen to be used as a foundation for the simulations performed in Chapter 5, Jee et al. (2001) and Yang et al. (1997). The choice of those two papers was based on the amount of information that they provided in terms of the bed specifications, isotherm parameters and main assumptions of the problem, which was significantly larger than the remaining papers screened.

2.4 Aspen Adsorption

After the literature review, it was confirmed that Aspen Adsorption is a widely used comprehensive flowsheet simulator for the analysis, design, simulation and optimization of several gas and liquid adsorption processes, for both industrial and laboratory scale. This software tool allows the simulation of ion exchange, liquid phase adsorption and gas phase adsorption processes with adsorption only or reactive gas adsorption processes where reaction and adsorption occur simultaneously [8].

This software package presents a different modelling approach, the gCSS simulation mode, to maximize profitability of periodic adsorption processes, such as PSA, TSA and VSA. Its models offer an effective design tool that can be more willingly used as an optimization package to determine optimal design and operating conditions for an adsorption process, based on the values of purity and recovery desired [5].

Nevertheless, other software packages are strong competitors, such as the gPROMS Process Builder, which provides advanced modelling capabilities that allow rapid and robust solving of cyclic separation systems, such as PSA units. It also supplies extensive libraries that allow easy construction and configuration of adsorption flowsheets and is considered and equation-oriented simulator [12].

3 Aspen Adsorption, an overview

Aspen Adsorption is a comprehensive flowsheet simulator for the analysis, design, simulation and optimization of adsorption processes. This software tool allows the simulation of ion exchange, liquid phase adsorption and gas phase adsorption processes and presents a different simulation mode for the simulation of cyclic processes such as Pressure Swing Adsorption, the gCSS mode.

In this chapter, an extensive analysis will be carried out, to understand and summarize the most important features of the software, from its necessary inputs to its possible outputs, acknowledging the main equations that rule adsorption and how they are solved using the available numerical methods. In order to do so, apart from a literature review, a series of tutorials and examples from Aspen's guidebooks [13-14] and from books on the subject [8] were performed.

The main sequential steps for every simulation using Aspen Adsorption are illustrated in Figure 2 and will be thoroughly discussed in the next sections.

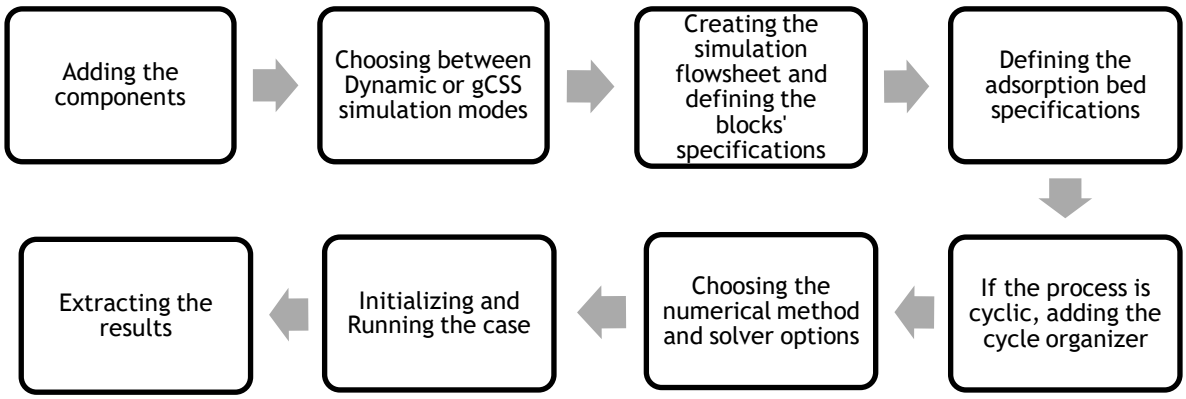


Figure 2 – Flow diagram for the main steps for a simulation in Aspen Adsorption.

3.1 Adding the components

The first task in the development of all simulation models is the addition of the components. There are two options for adding components to Aspen Adsorption: (i) importing them from Aspen Properties software, or (ii) using custom properties, input via a FORTRAN code, for example. The possibility of using Aspen Properties, with its embedded physical property and thermodynamic models' database is one of the advantages of using the Aspen Adsorption software. This option not only offers the opportunity of using a trustworthy and

complete database but also saves a lot of time. Nevertheless, the alternative way of introducing the components with custom properties is also available.

3.2 Choosing between Dynamic or gCSS simulation modes

Aspen Adsorption provides two simulation modes for gas phase adsorption processes: the gas Dynamic and gas CSS (gCSS) simulation mode. The choice of the simulation mode must be made in the beginning of the simulation because each mode has its own blocks and stream types, that although similar in terms of functionality and configuration, allow the software to perform different calculations.

The gCSS is specific for cyclic adsorption processes. When the adsorption process is cyclic, both simulation modes can be used (a comparison of their results is made in Chapter 4). However, when the adsorption process is not cyclic, for instance, for a breakthrough experiment, it is only possible to use the Dynamic simulation mode.

The main difference between the two simulation modes are the numerical methods that each mode uses to solve the differential and algebraic equations that represent the mass, momentum and energy balances, the kinetic and the equilibrium models. These numerical differences will be explained in detail in Section 3.6.

In addition to the differences in the numerical methods, different nomenclature is used for the blocks in the simulation flowsheet, as will be detailed in Section 3.3. In the cycle organizer, the only option available for gCSS simulations in the step change is time driven, as will be described in Section 3.5. Furthermore, the feed and product blocks are not available in this simulation mode, therefore, the temperature, pressure and molar compositions have to be specified directly in the streams and an initial value for the flowrates cannot be defined.

Lastly, it is important to highlight that the gCSS simulation mode offers a broader range of multi-component isotherm models when compared to the Dynamic mode.

3.3 Building the flowsheet and defining the blocks' specifications

In Aspen Adsorption, several libraries are available with models and stream types to simulate ion exchange, liquid phase adsorption and gas phase adsorption processes. In this work, the focus will be in gas phase adsorption, whose models can be found in Gas Dynamic and Gas CSS packages, as mentioned in Section 3.2.

Within these packages, the most commonly used models are the adsorption beds, named Gas_Bed in the Gas Dynamic and gCSS_Adsorber in the Gas CSS; the gas tank voids, Gas_Tank_Void in Gas Dynamic and gCSS_TankVoid in Gas CSS; the valves, Gas_Valve, in Gas Dynamic and gCSS_Valve in Gas CSS; the interaction units, Gas_Interaction in Gas Dynamic and

gCSS_Interaction in Gas CSS and finally, Gas_Feed and Gas_Product in Gas Dynamic with no equivalence in Gas CSS.

The Gas Bed (or gCSS_Adsorber) is used to rigorously model an adsorption bed. Since it characterizes the global adsorption process, it is the block that requires the most specifications, which will be described in detail on Section 3.4.

Gas Tank Voids (or gCSS_TankVoid) represent well-mixed tanks with configurable fixed volume and initial molar composition, pressure and temperature. They allow a large number of inlet and outlet streams and can be assumed adiabatic or non-adiabatic. The set of a Gas Bed with two Gas Tank Voids (one at its top and the other at its bottom) is a good representation of an adsorption column.

Gas Valves (or gCSS_Valve) are characterized by its coefficient (CV), which typically represents the ratio between the flowrate and the pressure drop through the valve. In Aspen Adsorption's usual problems, the valves are defined as Linear (flowrate is directly proportional do the pressure drop) or Pop (enable the control of the opening and closing pressure). However, they may also be configured as ISA (by the International Society of Automation standards) or Chocked. The valves may have four different configurations: completely closed (0), completely open (1), with a constant CV (2) or finally, with constant flowrate (3).

Gas Feed and Gas Product are model units used to represent the inlets and outlets of the process and can be manipulated to have the desired molar composition, pressure, temperature and flowrate. In the gCSS simulation mode, the feed and product's specifications are defined directly in the streams, since there is no specific block for them.

Gas Interaction units (or gCSS_Interaction) are used to store information such as flowrate, temperature, molar composition and pressure and can be instructed to replay that same information when necessary. The most frequent use for this unit, as will be further discussed, is found in cyclic processes such as Pressure Swing Adsorption, to act as a fictional second adsorbent bed.

All of the aforementioned models can have connections between them through Gas Material Connection Streams (or gCSS Connection Streams) and have initial default values to all required specifications. These models are presented in Figure 3, with the Gas Dynamic terminology.



Figure 3 – Main Aspen Adsorption's models with Gas Dynamic terminology.

3.4 Specifications of the adsorption bed

The Gas Bed model enables the modeling of the adsorption process and requires detailed specifications of the bed properties and the physical phenomena taking place. This block also allows the simulation of reactive gas adsorption processes where reaction and adsorption occur simultaneously.

3.4.1 The geometry window

The geometry window allows the user to introduce the specification of the number of layers of the adsorption bed, which represent individual and independent beds with their own set of assumptions (constant and initial values). This feature is typically applied when simulating a bed with more than one adsorbent material, where each layer represents an adsorbent with different properties.

The geometry of the bed might be set as vertical, horizontal or radial and in the first case, the spatial dimensions of the bed can be defined as 1D or 2D. In a 1D case, the second order spatial derivatives are evaluated only in axial direction, on the contrary, on a 2D case, they are evaluated in both axial and radial directions.

3.4.2 The adsorbent properties window

The most important properties of the adsorbents in each layer can be specified in the adsorbent properties window, namely its height (H_b), internal diameter (d_{bi}), particle radius (r_p), interparticle (ε_b) and intraparticle porosity (ε_p), bed density (ρ_b), particle density (ρ_p) and specific surface area (a_p). The units for each property may be designated.

3.4.3 Material and momentum balances window

The complete material balance for the adsorption bed, in a 1D model, is described in Equation (1). It consists of four main terms that represent the axial dispersion contribution, the convection, the gas phase accumulation and the adsorbed phase accumulation.

$$-D_{Li}\varepsilon_b \frac{\partial^2 C_i}{\partial x^2} + \frac{\partial (v_g C_i)}{\partial x} + \varepsilon_t \frac{\partial C_i}{\partial t} + \rho_b \frac{\partial Q_i}{\partial t} = 0 \qquad (1)$$

Here, D_{Li} represents the axial dispersion coefficient for component i, C_i represents the gas phase concentration for component i, and Q_i is the solid loading for component i. In order to complete the material balance, the following Equation (2) is required, where ρ_g stands for the gas density.

$$\sum_i C_i = \rho_g \tag{2}$$

The total bed porosity, ε_t, is the combined interparticle and intraparticle porosity and it is calculated from Equation (3). The bed density, ρ_b, is calculated from Equation (4).

$$\varepsilon_t = \varepsilon_b + \varepsilon_p(1 - \varepsilon_b) \tag{3}$$

$$\rho_b = \rho_p(1 - \varepsilon_b) \tag{4}$$

If the axial dispersion term is inactive, plug flow is considered. On the contrary, if this term is not negligible, it is necessary to provide values of the axial dispersion coefficient for all components. These values can be assumed constant and provided by the user, or, in case they vary along the bed, they are estimated from correlations of the software. The third and last option is to provide a FORTRAN routine, for example, that estimates the coefficient's variation.

Regarding momentum balances, there are two main options for an adsorption bed: constant pressure, meaning that the bed is driven by gas superficial velocity, or pressure driven, meaning the velocity is related to pressure gradients. In the first one, both pressure and velocity can be kept constant and it should only be used for breakthrough investigations. In the second one, several well-known equations can be chosen to model the pressure drop along the bed. For laminar flow, it is possible to use Darcy's Law (linear relationship between the gas superficial velocity and the pressure gradient) or Karman-Kozeny equation; for turbulent flow, Burke-Plummer equation is available, otherwise the most general option, Ergun equation (combines Karman-Kozeny in the first term and Burke-Plummer in the second term), described in Equation (5), can also be chosen.

$$\frac{\partial P}{\partial x} = -\left(\frac{150\times10^{-5}\mu_g(1-\varepsilon_b)^2}{(2r_p\Psi)^2\varepsilon_b^3}v_g + \frac{1.75\times10^{-5}M_w\rho_g(1-\varepsilon_b)}{2r_p\Psi\,\varepsilon_b^3}v_g^2\right) \tag{5}$$

Here, μ_g represents the gas mixture viscosity, r_p is the particle radius, Ψ is the particle shape factor, v_g represents the superficial gas velocity and M_w stands for the molecular weight of the gaseous mixture.

3.4.4 Kinetics (Resistances to mass transfer) window

Typically, several mass transfer resistances exist in gas phase adsorption processes from the resistances between bulk gas phase and gas-solid interface, to resistances due to the porous structure of the adsorbent, particularly, if the adsorbent has two distinct pore size regions.

These resistances can be subdivided to account separately for macropore and micropore resistances.

In this section, the first thing to choose is whether the mass transfer driving force is a function of the solid phase loading or the gas phase concentration. Afterwards, it is possible to choose a Lumped Resistance model, where the separate resistances to mass transfer are lumped as a single overall factor. Generally, it is more convenient to depict the transfer rate in terms of a lumped resistance coefficient rather than to use a diffusion equation to represent adsorption, although in this software, this last option is also available but will not be addressed. Aspen Adsorption presents two approximations to the lumped resistance model: Linear Driving Force approximation (LDF) and Quadratic Driving Force approximation (QDF), described, respectively, in Equations (6) and (7) for fluid and solid.

$$Fluid: \rho_b \frac{dQ_i}{dt} = k_{Fi}(C_i - C_i^*) \qquad Solid: \frac{dQ_i}{dt} = k_{Si}(Q_i - Q_i^*) \tag{6}$$

$$Fluid: \rho_b \frac{dQ_i}{dt} = k_{Fi}\frac{(C_i)^2-(C_i^*)^2}{2C_i} \qquad Solid: \frac{dQ_i}{dt} = k_{Si}\frac{(Q_i)^2-(Q_i^*)^2}{2Q_i} \tag{7}$$

Here, C_i^* and Q_i^* represent the equilibrium gas phase concentration and equilibrium solid loading for component i, respectively. The mass transfer coefficients, k_{Fi} and k_{Si}, can be assumed constant and provided by the user, or they can vary and, in that case, are either estimated by the software's correlations or by a user-provided subroutine (for example FORTRAN).

3.4.5 Equilibrium (Isotherm) window

Adsorption is the term given to the tendency of molecules from a fluid phase to stick to the surface of a solid. The adsorption process is modeled by an isotherm, which describes the amount of each component adsorbed into the solid at thermodynamic equilibrium, as a function of pressure or concentration and temperature. Knowing the adsorption isotherms for the feed components, it is possible to predict the performance of the adsorbent bed for the specified operating conditions, which represents a crucial step in the design and simulation of adsorption processes.

A wide range of isotherm models is available in this section for either pure components or multi-component mixtures. However, to simulate most real cases, it is more relevant to consider the adsorption equilibria of the mixture, rather than pure components, since individual gas components adsorb in a different way when mixed with other components. It is common practice to predict mixture isotherms from pure component isotherms such as Langmuir, Freundlich, Henry, Toth and Volmer models. Several methods for predicting mixture isotherms from these pure component isotherms have been proposed, for instance the Extended Langmuir

approach and the Ideal Adsorbed Solution (IAS), also available in this software. It is also possible to provide user-defined isotherms through FORTRAN subroutines, for example.

Given the importance of this particular section, it is recommended, before any simulation, to carefully adjust experimental parameters to the available isotherms of the software or even, dedicate some time to test and understand which of the available isotherm models better represents the case study that will be simulated.

Finally, the isotherms can be expressed as function of partial pressures or concentrations, and in some cases also as a function of temperature. It is relevant to note that the input forms for the isotherms must obey to a specific set of units, as detailed in Table 1.

Table 1 - Set of units considered by Aspen Adsorption in isotherm parameters

Variable	Unit of measurement
Solid loading ($\boldsymbol{Q_i}$)	kmol/kg
Gas phase concentration ($\boldsymbol{C_i}$)	kmol/m^3
Pressure ($\boldsymbol{P}$)	bar
Temperature ($\boldsymbol{T}$)	K

3.4.6 Energy Balance window

In this section, the first option to be made is whether the problem is isothermal or non-isothermal. In the first case, the energy balance will not be necessary since the gas and solid temperatures will be held constant and equal. When the problem is considered non-isothermal, energy balances are performed for the fluid and solid phases and besides that, if the bed is considered non-adiabatic, an extra energy balance will be implemented for its wall.

Depending on their relevance for the simulated case, some of the terms may not be considered in the balances, for instance, the software allows the consideration of the system as non-isothermal with no conduction (where axial thermal conduction terms are negligible) or non-isothermal with solid and/or gas conduction (where these axial thermal conduction terms are considered in the balances). Similarly, in the solid phase balance, the user is able to set the enthalpy of adsorption term as negligible, if appropriate, and in the wall energy balance, a thin wall assumption can be made, where the conductivity and heat accumulation along the wall are neglected.

The energy balance for the fluid phase, in a 1D model, is represented by Equation (8) and consists of the following six terms: axial thermal conduction, convection, P-V work

compression, thermal accumulation in the gas phase, heat transfer between gas and solid and heat transfer between gas and the internal wall of the adsorber.

$$-k_g \varepsilon_b \frac{\partial^2 T_g}{\partial x^2} + C_{vg} v_g \rho_g \frac{\partial T_g}{\partial x} + P \frac{\partial v_g}{\partial x} + C_{vg} \rho_g \varepsilon_t \frac{\partial T_g}{\partial t} + H_s a_p (T_g - T_s) + H_w \frac{A_{Hi}}{V_{Hi}} (T_g - T_w) = 0 \quad (8)$$

Here T_g, T_s and T_w represent the gas, solid and wall temperatures, k_g is the gas mixture thermal conductivity, C_{vg} stands for the gas mixture heat capacity, P represents the pressure, H_s and H_w stand for the fluid/solid heat transfer coefficient and the fluid/wall heat transfer coefficient, a_p is the particle external surface area to particle volume ratio, A_{Hi} and V_{Hi} represent the internal wall element area and the internal wall element volume for heat transfer.

The energy balance for the solid phase, in a 1D model, is represented in Equation (9) and considers the following four terms: axial thermal conduction, thermal accumulation in the solid phase, thermal accumulation by the enthalpy of adsorption and heat transfer between gas and solid.

$$-k_s \frac{\partial^2 T_s}{\partial x^2} + C_{Ps} \rho_b \frac{\partial T_s}{\partial t} + \rho_p \sum_i \left(\Delta H_i \frac{\partial Q_i}{\partial t} \right) - H_s a_p (T_g - T_s) = 0 \quad (9)$$

Here, k_s represents the solid phase thermal conductivity, C_{Ps} is the solid heat capacity and ΔH_i stands for the enthalpy of adsorption for component i.

Finally, for the wall energy balance, considering a 1D model, the following four terms can be incorporated: axial thermal conduction along the wall, thermal accumulation in the wall material, heat transfer between gas and wall and heat transfer between wall and the surrounding environment.

$$-k_w \frac{\partial^2 T_w}{\partial x^2} + C_{Pw} \rho_w \frac{\partial T_w}{\partial t} - H_w \frac{A_{Hi}}{V_{Ho}} (T_g - T_w) + H_{amb} \frac{A_{Ho}}{V_{Ho}} (T_w - T_{amb}) = 0 \quad (10)$$

Here, k_w is the wall thermal conductivity, C_{Pw} represents the wall material heat capacity, ρ_w is the wall material density, H_{amb} stands for the wall/environment heat transfer coefficient, A_{Ho} and V_{Ho} represent the external wall element area and the external wall element volume for heat transfer, finally T_{amb} is the environment temperature.

The parameters presented in the fluid, solid and wall energy balances, such as heat capacities, heats of adsorption and heat transfer coefficients are either constant and provided by the user or estimated by the software. Nevertheless, there is always the option of providing a subroutine to infer these parameters (for example FORTRAN).

3.4.7 Reaction window

Finally, the last window of the Gas Bed model enables the configuration of reactive gas adsorption processes where reactions (homogeneous or heterogeneous) and adsorption occur simultaneously. However, as the present study focused on PSA units, this window was not explored in detail.

3.5 Adding the cycle organizer

When simulating a simple adsorption case, the previous steps are enough to define the problem. In cyclic adsorptive processes such as Pressure Swing Adsorption, another feature has to be added to the simulation flowsheet: the Cycle Organizer, presented in Figure 4.

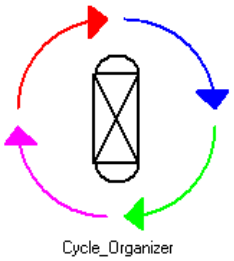


Figure 4 - The cycle organizer.

Using this tool, the cycle that the bed will go through can be defined. First, the number of steps in the cycle must be designated, and after naming each step, the manipulated variables in each one can be chosen. These manipulated variables can go from valve specifications (in order to control whether they are closed, open, have a constant flowrate through them or a constant CV), pressure and temperature values at a given block, among others.

After defining each step, it is then necessary to instruct the software when to change from each step to the next. For this part, there are three main options: either the step change is time driven (each step has a specified time duration), event driven (the software is instructed to change to the next step whenever a defined variable is superior, inferior or equal to a certain value or whenever a defined variable is above or beyond a certain specified range) or step dependent (meaning a step will have the same duration as the step that it depends on). Using the gCSS simulation mode, the only option available for the step change is for it to be time driven.

An additional option in the Cycle organizer is to use the Interaction feature, which is available when the flowsheet has a Gas Interaction unit. In this section, it is possible to instruct this block when to record and replay information from the Gas Bed allowing it to act as a fictional second bed, with the exact same configurations as the first one. This particular feature

will be addressed in detail in the next chapter when discussing the possible configurations for PSA simulations in Aspen Adsorption.

Finally, the maximum number of cycles can also be set.

3.6 Choosing the numerical methods and solver options

As described in the previous section, Aspen Adsorption uses a set of partial differential equations (PDE), ordinary differential equations (ODE) and algebraic equations that represent the mass, momentum and energy balances, the kinetic and the equilibrium models, which, with the appropriate initial and boundary conditions, describe the adsorption process.

Spatial derivatives are discretized over a fixed uniform grid (2D) or number of nodes (1D) given by the user, and the resulting system of differential and algebraic equations must be solved simultaneously since they are coupled. In order to transform PDE into a system of ODE, the method of lines is applied, represented in Figure 5. It consists of discretizing the spatial derivatives, while keeping one continuous variable constant (usually time), it is as if the dependent variables at each node march in time, along parallel lines perpendicular to the spatial axis.

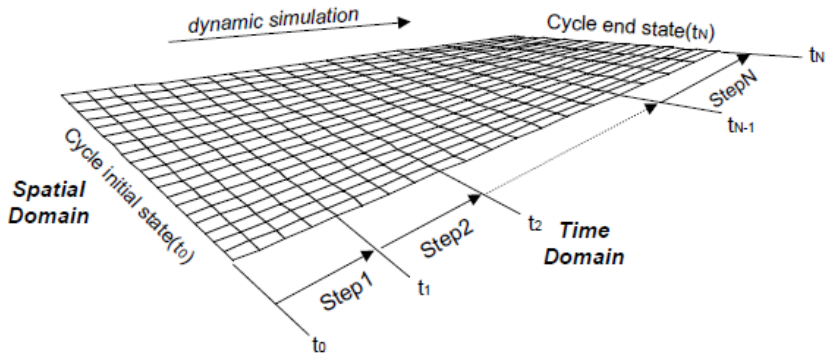


Figure 5 - Visual representation of the Method of Lines [13].

In Dynamic mode, several discretization methods are available from Upwind, Central, Quadratic, Biased-Upwind and Mixed Differencing Schemes (Appendix B). The recommended options mentioned on the Aspen Adsorption Reference Guide [13] for better accuracy, stability and simulation time are the Upwind Differencing Scheme, Quadratic Differencing Scheme or Mixed Differencing Scheme. In cases when the adsorption isotherm is highly nonlinear, it is recommended to use the Biased Upwind Differencing Scheme or the Flux Limiter methods [13].

Aspen Adsorption also presents a different simulation mode for cyclic processes like Pressure Swing Adsorption units, the gCSS simulation mode. A periodic adsorption process consists of a sequence of steps in each cycle and, after a given number of cycles, the conditions at the end of the cycle are equal to those at the beginning, meaning the performance of the separation unit is considered constant. This point is designated the Cyclic Steady State (CSS).

Traditionally, to determine the CSS, a dynamic simulation of the system is required and, when a defined criterion is confirmed, for instance, the variation of the product purity is below a certain percentage or the cycle initial state is identical to the cycle end state, it is considered that the maximum performance of the unit was achieved.

The existence of a Cyclic Steady State lead to the development of different numerical methods. These methods replace the initial condition by a periodicity condition, requiring that the system state at the end of each cycle is identical to its beginning. Hence, this constrains the system within a specified time domain length, from the starting to the ending point of a cycle. Consequently, a steady state simulation is feasible by complete discretization of space and time within a confined time length. A visual representation of this method is exhibited in Figure 6.

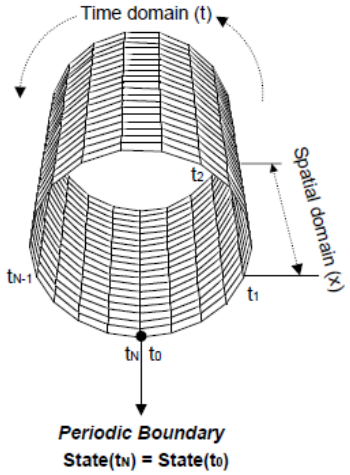


Figure 6 - Visual representation of the discretization method available in gCSS mode [13].

Thus, using the gCSS simulation mode, it is possible to directly determine the cyclic steady state of a system, and then, if desired, execute a dynamic run, using the cyclic steady state conditions as the initial ones, improving convergence in highly nonlinear problems.

Nonetheless, using the gCSS simulation mode, it is also possible to execute a dynamic run without the previous determination of CSS, in case it is more relevant to understand the system's evolution rather than its maximum performance. In this type of simulations, the main difference between using the Dynamic simulation mode and the gCSS simulation mode, is the discretization methods available, which, in gCSS mode, are Central Finite Differences or Orthogonal Collocation on Finite Elements (Appendix B)

Besides the discretization methods, which depend on the chosen simulation mode, as described above, the solver options on both simulation modes are configurable. Different approaches for non-linear solvers (such as Newton and Fast Newton) and integrators (such as Implicit and Explicit Euler) should be tested and the tolerances and step sizes should be adjusted to optimize the results.

3.7 Initializing, running and extracting the results

When the problem is completely defined and the numerical methods are chosen, it is possible to initialize and run the simulation. When the run stops, the results of the simulation can be extracted.

The results can be plotted in time series plots or profile plots. The first ones describe the variation on any chosen variables at a given point during the simulation's time. On the other hand, the profile plots describe the variation of variables along the discretization nodes at any given time.

The profile plots can also be manipulated to present the correlation between any given variable in X-axis with another one in the Y-axis and even a third axis can be added, creating a 3D plot. Figure 7 presents an example of a 2D plot (left), showing the evolution of the molar fractions of two components (O_2 and N_2) in the product stream during a PSA simulation and a 3D plot (right), representing the pressure variation along the bed length and time during a PSA simulation.

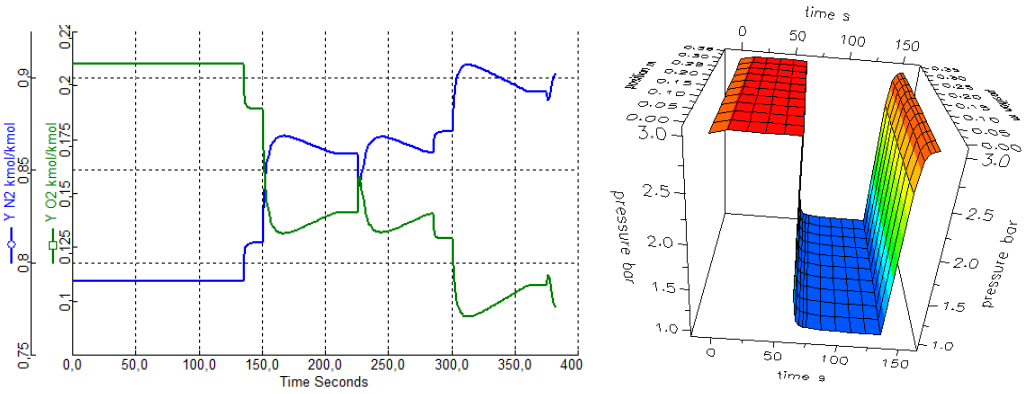


Figure 7 - Example of a 2D and a 3D plot from Aspen Adsorption.

Both types of plots can be edited in the software, or, if preferred, the data can be extracted as a table and post-processed on other software tools.

4 Simulation of a PSA unit using Aspen Adsorption

This chapter presents the studies performed for Pressure Swing Adsorption processes using Aspen Adsorption software package. The case study is one of Aspen Adsorption's Training Manual examples [14], a PSA unit for air separation, which will be presented in detail in Section 4.1. To go deeper in understanding how adsorption and desorption are simulated, to know the assumptions made by the software and to find some critical details, a two-step cycle was simulated on a single bed. This study is presented in Section 4.2.

Aspen Adsorption's guidebooks [13-14] recommend two approaches for PSA simulations, here designated by Model 1 and Model 2, respectively. Using the same case study, both approaches were compared and an equivalence between them was established in Section 4.3. Lastly, in Section 4.4, the same case study was simulated, using different simulation modes, Dynamic and gCSS.

4.1 The case study

The case reported is a PSA unit for air separation, considering an approximation on the air composition of 21% O_2 and 79% N_2. The separation takes place on a Carbon Molecular Sieve (CMS) adsorbent bed and the main assumptions of the simulation are: (1) Peng-Robinson model was used as equation of state (specified when choosing the components from Aspen Properties); (2) In the material balance, the axial dispersion term was neglected (plug flow approximation); (3) For the momentum balance, Ergun Equation was used; (4) A linear lumped resistance to mass transfer was considered (LDF model); (5) The system was considered as isothermal (no energy balance); (6) In terms of geometry, the adsorbent bed is vertical with a single layer containing the CMS adsorbent; (7) A 1D discretization with 20 nodes was considered using the Biased Upwind Differencing Scheme as discretization method.

The isotherm, which described the adsorption process was Extended Langmuir 1 with concentration dependency, represented in Equation (11) and the parameters for each component are listed on Table 2. The remaining specifications are listed on Table 3.

$$Q_i = \frac{IP_{1i}C_i}{1+\sum_k (IP_{2k}C_k)} \tag{11}$$

Table 2 - Isotherm parameters for each component

	N_2	**O_2**
IP_1 (m^3/kg)	9.0108 x 10^{-3}	9.3652 x 10^{-3}
IP_2 (m^3/kmol)	3.3712	3.5038

Table 3 - Specifications of the case study

Parameter	Value
Bed height, H_b (m)	0.350
Bed internal diameter, d_{bi} (m)	0.035
Bed porosity, ε_b	0.400
Particle density, ρ_p (kg/m^3)	592.6
Particle radius, r_p (m)	1.050 x 10^{-3}
Solid mass transfer coefficient for N_2, k_{SN2} (1/s)	7.605 x 10^{-3}
Solid mass transfer coefficient for O_2, k_{SO2} (1/s)	4.476 x 10^{-2}

The feed flowrate consists in a mixture with molar fractions of 79% N_2 and 21% O_2, at 3.045 bar and 298.15 K, and molar flowrate of 5 x 10^{-7} kmol/s, which corresponds to a volumetric flowrate of 4,078 x 10^{-6} m^3/s, at the feed's pressure and temperature conditions. The adsorbent bed and the tanks in the simulation were initially filled with feed. The pressure considered for the product streams was 1.013 bar.

4.2. Two-step cycle on a single bed

A two-step cycle simulation was run before the study of the complete PSA unit with the purpose of understanding the assumptions and calculations executed by the software tool during the adsorption and desorption steps. The process flowsheet of this simulation is represented in Figure 8.

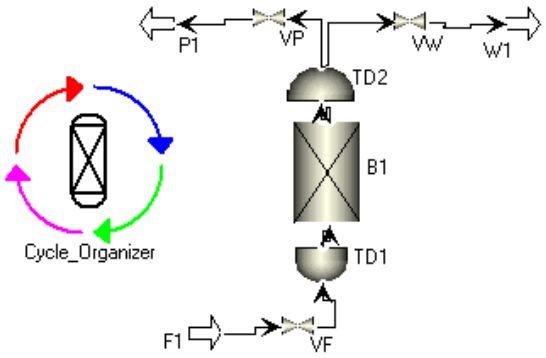


Figure 8 - Process flowsheet of the two-step cycle simulation on a single bed.

The simulation flowsheet was composed of an adsorption bed, B1 with specifications given in Tables 2 and 3, two tank voids, TD1 and TD2, three valves, VP, VW and VF with the purpose of controlling the flowrate through the Feed (F1), the Product (P1) and the Waste (W1) and a Cycle Organizer to control the cycle's steps.

To replicate the adsorption step, during the first step of the cycle, both VF and VP valves were open, and VW was closed. VF was completely open and VP had a constant flowrate of 5.2 x 10^{-9} kmol/s, which corresponds to a volume flow rate of 1.27 x 10^{-7} m^3/s, at 1 atm and 298.15 K. In the second step, both VF and VP valves were closed, and VW was open with a constant CV of 6 x 10^{-6} kmol/s/bar. A summary of the cycle is listed in Table 4, including the valve's specification for each case.

Table 4 - *Summary of two-step cycle's configurations*

	Step 1: Adsorption	**Step 2: Desorption**
VF	Completely open (1)	Closed (0)
VP	Open with a constant flowrate (3)	Closed (0)
VW	Closed (0)	Open with a constant CV (2)
Duration (s)	1000	1000

After simulating two full cycles, some conclusions were made on how adsorption and desorption are simulated on Aspen Adsorption. Primarily, a material balance of each component, *i*, was confirmed according to Equation (12).

$$\int_{t_{start}}^{t_{end}}(F_{F1}y_{iF1})dt - \int_{t_{start}}^{t_{end}}(F_{P1}y_{iP1} + F_{W1}y_{iW1})dt = \left(Q_{i_{tend}} - Q_{i_{tstart}}\right)m_{ads} + \left(C_{i_{tend}} - C_{i_{tstart}}\right)V_{bulk} \quad (12)$$

The material balance was independently calculated for each step of the cycle; t_{start} represents the time at which the step starts and t_{end} the time at which the step ends; F_{F1}, F_{P1}, F_{W1} are the molar flowrates of the streams F1, P1 and W1, respectively; y_{iF1}, y_{iP1}, y_{iW1} are the molar fractions of component *i* on streams F1, P1 and W1, respectively; $Q_{i_{tend}}$, $Q_{i_{tstart}}$ represent the solid loading of component *i*; $C_{i_{tend}}$ and $C_{i_{tstart}}$ represent the gas phase concentration for component *i*; V_{bulk} is the volume of the bulk and finally, m_{ads} stands for the mass of adsorbent. The values for the flowrates and molar compositions were extracted from the software in form of a table, with values for each second.

4.2.1 Analysis of cycle 1

Starting with the first cycle, on step 1, since the bed was previously filled with feed, no adsorption occurs, therefore, the amount of each component that enters through VF and leaves the bed through VP is equal. There is no accumulation and the solid loading is constant, equal to the initial value during the entire step duration. On step 2, only VW is open and, as the bed depressurizes, the solid loading decreases since desorption is taking place. The calculated amount of component that exits in W1 is approximately equal to the amount of component

desorbed in the same time period. For N_2, these values are respectively, 6.20 x 10^{-5} kmol and 5.90 x 10^{-5} kmol.

4.2.2 Analysis of cycle 2

On step 1 of the second cycle, the bed is pressurized, and adsorption begins. During this step, the calculated amount of component accumulated is approximately equal to the amount held back in the solid and the bulk, which for N_2 is respectively, 6.15 x 10^{-5} kmol and 5.75 x 10^{-5} kmol. Finally, on step 2, the calculated amount of N_2 that exits in W1, 6.50 x 10^{-5} kmol, is approximately equal to the amount of N_2 desorbed, 6.18 x 10^{-5} kmol.

The errors associated with these calculations were caused by some accumulation in the tank voids during these steps. Two integration methods were used, the trapezoidal rule and the Simpson 1/3 rule, directly applied to the data extracted from Aspen Adsorption.

With the material balance checked, some other details were observed during this simulation. The first noticed situation was that the software estimates a value for the product composition, even when the flowrate of the product is zero. In this case, during step 2 (1000-2000 s and 3000-4000 s), the VP valve was closed, no flow was passing through it, but the software estimated an exit composition equal to the tank TD2, which is also equal to the exit composition in W1. The variation of the P1 stream flowrate and the P1 stream N_2 and O_2 molar fractions are represented in Figure 9 and 10, respectively.

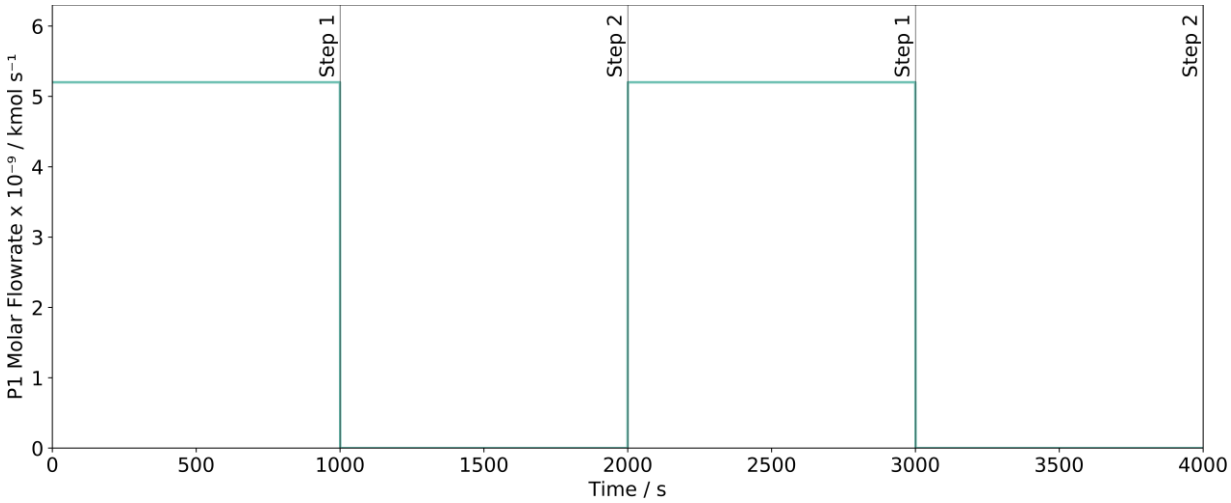


Figure 9 - Variation of the Product (P1) flowrate.

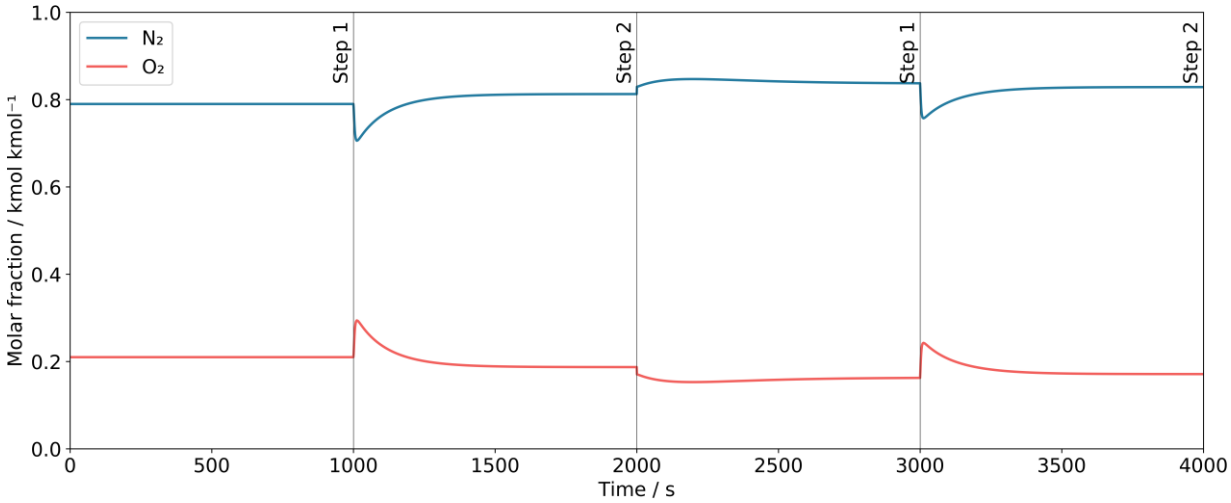


Figure 10 - Variation of O_2 and N_2 molar fractions in the product stream (P1).

In Figure 10, it is also possible to notice that, when the desorption step begins (at time equal to 1000 s), the O_2, which was mostly held in the solid, is released and its molar fraction in the tank TD2 (equal to P1 as mentioned) increases and, during the adsorption step, the opposite happens, decreasing its molar fraction and increasing the N_2 purity.

Finally, an additional particularity of the software was discovered regarding the functioning of the linear valves used in this simulation. It was found that in step 2 (1000 s – 2000 s), when VW is open with a constant CV, the upstream and downstream pressures of the valve never reach an equal value, which occurs frequently in reality after some time. Since the CV is the ratio between the flowrate through the valve and its ΔP, if ΔP never reaches zero, W1 flowrate is never null during step 2, as demonstrated in Figure 11. This could be a useful feature since the software assumes there is always some pressure difference, even if it is extremely small, driving the flow. In this case, at the end of step 2, the pressure difference was 3.22 x 10^{-5} bar, which, with a CV of 6 x 10^{-6} kmol/s/bar, results in a very small flowrate of 1.93 x 10^{-10} kmol/s.

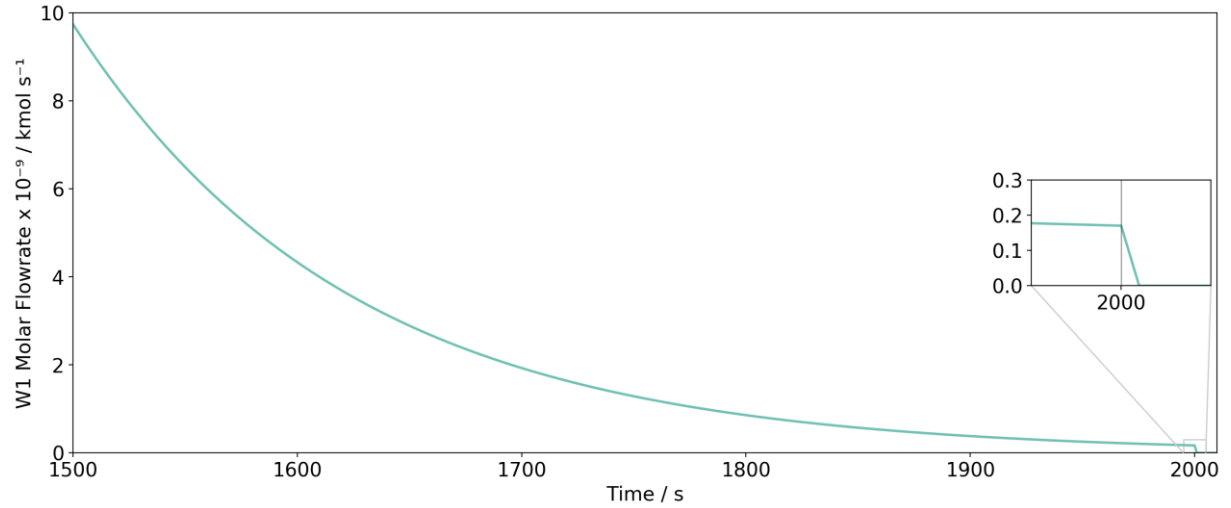


Figure 11 - Variation of the Waste (W1) flowrate during the desorption step.

Different values were tested for the CV of this valve and it was concluded that with CVs higher than 10^{-3}, some numerical errors might happen, and negative values for the flowrate and ΔP might occur in order to uphold the CV of the valve constant. This occurrence causes errors and damages the adsorption bed's performance since it is reversing the flow direction. A solution was found that consists of using a control action in the valve, forcing the flowrate and ΔP to be null instead of assuming negative values. This feature is available in every linear valve with the name "Apply stop action", and by activating it, the threat of reversing the direction of the flow is eliminated.

As mentioned before, when the flowrate is null, the molar fraction is estimated as being equal to the previous block's molar fraction. In order to obtain accurate values, a cooperative examination of both flowrates and molar fractions is always recommended so that it is known when these values are being estimated and when they truly represent reality.

Before starting a complete PSA simulation, the breakthrough curve, illustrated in Figure 12, was also analyzed. The analysis of this curve before a PSA simulation is relevant since it provides a realistic estimation of the adsorbent's performance. For this part of the simulation, valves, tanks and stream W1 were eliminated, and the feed (F1) and the product (P1) streams were directly connected to the adsorption bed, which was previously filled with pure N_2. The molar fractions of N_2 and O_2 were collected in P1.

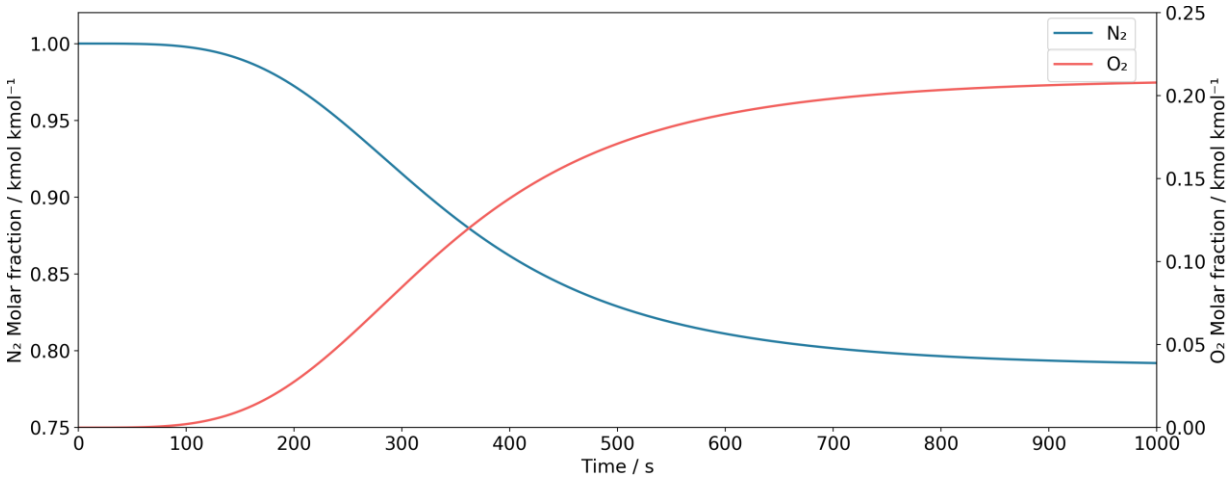


Figure 12 - Breakthrough curve.

From the analysis of the breakthrough curve, it is possible to conclude that the maximum performance of the bed is guaranteed during approximately 80 s. After that, the bed is fully saturated and since the O_2 in the feed stream cannot be adsorbed anymore, its concentration in P1 stream increases. Thus, the adsorption step, in this case, should not be longer than 80 s.

4.3. Two models for PSA simulations

For the simulation of a PSA unit, two approaches were tested: Model 1 and Model 2. Both PSA units operate according to a Skarstrom cycle with four main steps: adsorption, blowdown, purge and pressurization. The step's duration is 60 s for purge and adsorption steps (1,3) and 15 s for pressurization and blowdown steps (2,4). The Model 1, represented in Figure 13, is closer to the configuration of a real PSA unit, described on the State of the Art.

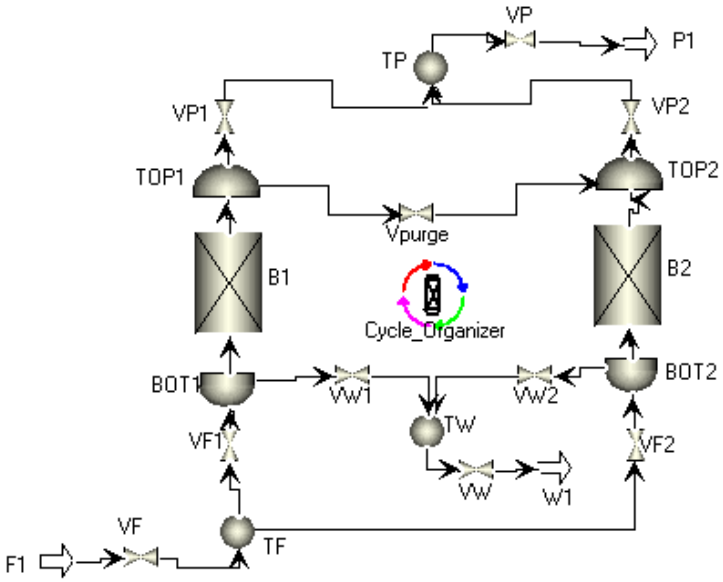


Figure 13 - Simulation flowsheet for Model 1.

This model consists of two identical adsorption beds (B1 and B2), each with two tanks (TOP1, BOT1, TOP2, BOT2), four main valves (VF, VP, VW and VPurge), six intermediate valves (VF1, VF2, VP1, VP2, VW1 and VW2) and three tanks to allow the division and union of streams (TF, TP and TW). The specifications of the cycle for this model are listed on Table 5, and were extracted from the example used for this study [14].

The cycle consists of the following four steps: 1) adsorption in B1 and purge in B2, 2) blowdown in B1 and pressurization in B2, 3) purge in B1 and adsorption in B2, 4) pressurization in B1 and blowdown in B2.

Table 5 - Specifications of the cycle for Model 1

	Step 1: Adsorption B1, Purge B2	Step 2: Blowdown B1, Pressurization B2	Step 3: Purge B1, Adsorption B2	Step 4: Pressurization B1, Blowdown B2
VF	1	1	1	2 (CV=1.4 x 10^{-5} kmol/s/bar)
VF1	1	0	0	1
VF2	0	1	1	0
VPurge	2 (CV=1.8 x 10^{-7} kmol/s/bar)	0	2 (CV=1.8 x 10^{-7} kmol/s/bar)	0
VP	3 (F=5.2 x 10^{-9} kmol/s)	3 (F=5.2 x 10^{-9} kmol/s)	3 (F=5.2 x 10^{-9} kmol/s)	3 (F=5.2 x 10^{-9} kmol/s)
VP1	1	0	0	1
VP2	0	1	1	0
VW	2 (CV=1.0 x 10^{-5} kmol/s/bar)	2 (CV=6.0 x 10^{-6} kmol/s/bar)	2 (CV=1.0 x 10^{-5} kmol/s/bar)	2 (CV=6.0 x 10^{-6} kmol/s/bar)
VW1	0	1	1	0
VW2	1	0	0	1

The Model 2, an approximation of the first model, represented in Figure 14, consists of one Gas Bed (B1) with two tanks (TD1 and TD2) connected to a Gas Interaction unit (D1) and 4 valves VF, VP, VW and VD to control the flowrates.

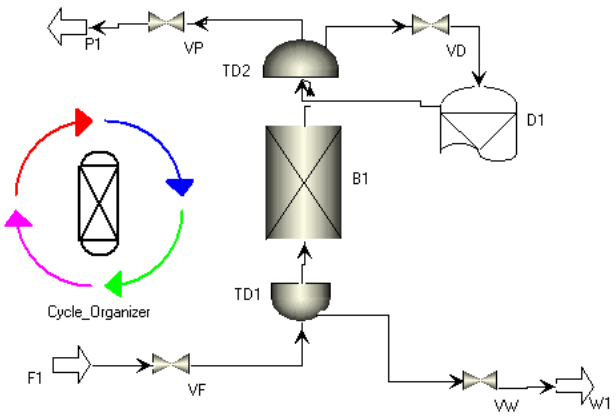


Figure 14 - Simulation flowsheet for Model 2.

As mentioned in Chapter 3, the Gas Interaction unit is able to store and replay data such as temperature, molar composition, pressure and flowrates, therefore, in this model, D1 acts as a fictional second bed, with the exact same behavior as B1. In the cycle organizer, D1 is instructed to store information from B1 during the adsorption step and then replay it in the step where a second bed would be adsorbing. It is important to emphasize that this model can

only be used if the adsorption beds, in the case to be simulated, are identical with exactly the same specifications.

The specifications of the cycle for this model, which used a gas-interaction fictional unit, are listed on Table 6. The cycle consists of the following four steps: 1) adsorption in B1 and purge in D1, 2) blowdown in B1, 3) purge in B1 and adsorption in D1, 4) pressurization in B1. Steps 1 and 3 are linked in the cycle organizer through an interaction so that the information from B1 stored in D1, can be re-sent to the tank void on top of B1 during these steps. Pressurization and blowdown in D1 are not required since it would not improve its performance; the only specified variable for this block is the minimum pressure of 1.013 bar. The values of the flowrates and CVs were given by the tutorial from Aspen Adsorption's Training Manual, used for this study [14].

Table 6 - Specifications of the cycle for Model 2

	Step 1: Adsorption B1, Purge D1	**Step 2: Blowdown B1**	**Step 3: Purge B1, Adsorption D1**	**Step 4: Pressurization B1**
VF	1	0	0	2 (CV=1.4 x 10^{-5} kmol/s/bar)
VD	2 (CV=1.8 x 10^{-7} kmol/s/bar)	0	0	0
VP	3 (F=5.2 x 10^{-9} kmol/s)	0	0	0
VW	0	2 (CV=6.0 x 10^{-6} kmol/s/bar)	2 (CV=1.0 x 10^{-5} kmol/s/bar)	0
Interactions	3	-	1	-

The results of the product (P1) N_2 molar composition after 15 cycles are represented in Figure 15.

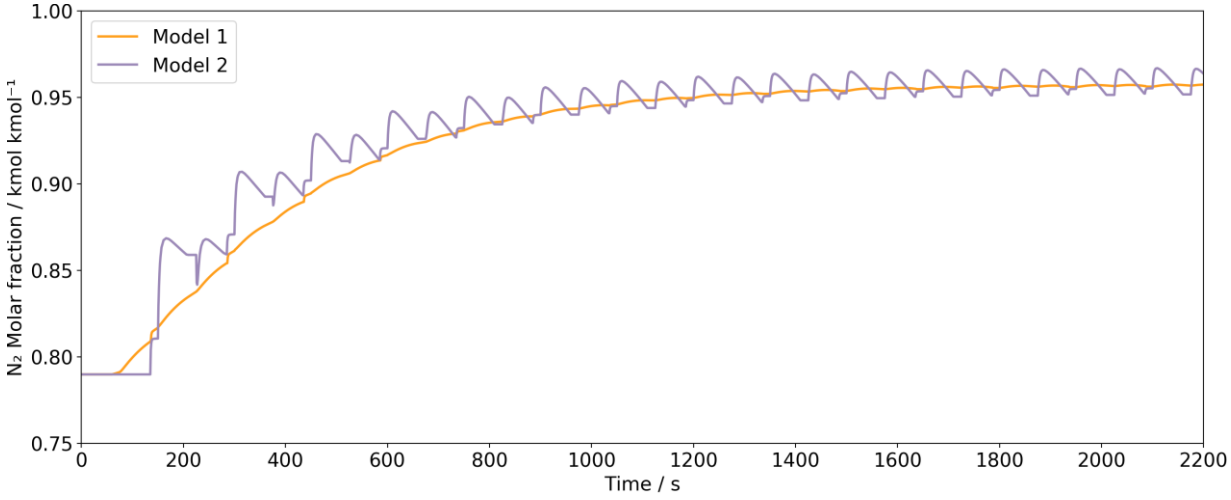


Figure 15 - N_2 molar fraction in P1 for Model 1 and 2 during 15 cycles.

Two main differences between the model's results were straightforwardly noticed. Foremost, the delay of the second model's results compared to the first model's results and, evidently, the difference in the shape of the curves.

In order to have a deeper understanding of the lag between the curves, the first two cycles, represented in Figure 16, were analyzed.

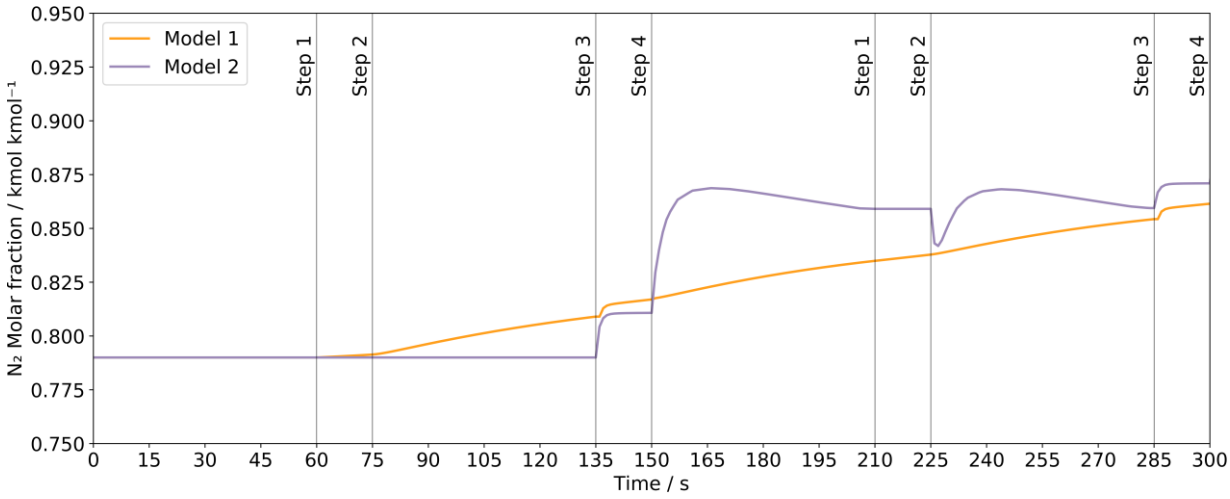


Figure 16 - N_2 molar fraction in P1 for Model 1 and 2 during the first 2 cycles.

As verified in Figure 16, during the first step (60 s), the N_2 molar fraction in the product stream is constant in both models since the bed was initially filled with the feed stream. At this step, in Model 1, B1 is at higher pressure, during an adsorption type step, but B2 is at lower pressure being purged and discharged to the environment. During step 2 (60-75 s), in the first model, B2 is pressurized and since it has already been purged in the previous step, a driving force exists and, adsorption slowly begins as the pressure rises inside the bed and the N_2 molar fraction in the product starts to increase and continues during adsorption on step 3 (75-135 s).

On the other hand, in the second model, during step 1 of the first cycle, the fictional unit, D1, stores the values from B1, which will only be replayed in step 3, sending the information as if D1 was saturated with the feed. During step 2 and 3, B1 is going through a blowdown and purge, respectively, so, no adsorption is expected. As D1 can only store and replay information from B1, no adsorption occurs on the first three steps of the cycle. It's only on step 4, when B1 is being pressurized, that Model 2 exhibits a boost in N_2 molar fraction. The fact that D1 can only act as a fictional bed, storing and replaying data, is the explanation for the lag between the two models.

Justifying the difference between the shape of the curves in the two models required a deeper study of the differences between the model's functioning. When comparing the compositions of the TD2 block and TOP1 and TOP2 blocks, the same shape of the curve was found, since all of these blocks represent the tank above an adsorbent bed that is going through

the same cycle. These compositions are represented in Figure 17. The lag between the models, explained before, is also verified.

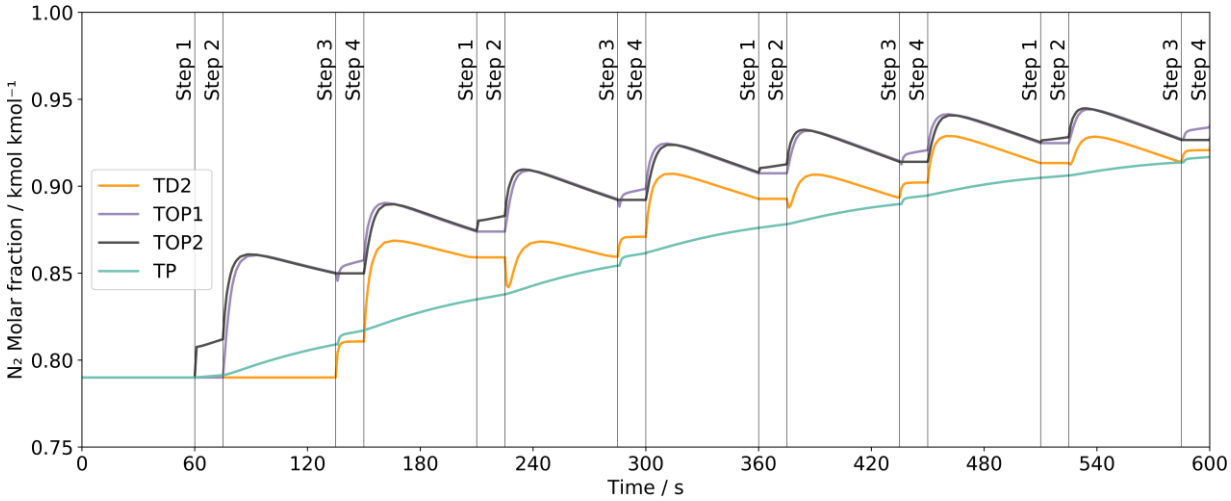


Figure 17 - N_2 molar fraction in TD2, TOP1, TOP2 and TP during the first 4 cycles.

In the second model, the product stream is directly connected to the tank TD2, and during steps 2, 3 and 4, VP is closed, so the composition in the product stream is estimated as being the same as the composition in TD2. In this case, this approximation of the software is extremely useful because in order to execute the blowdown, purge and pressurization of B1, VP has to be closed. On the contrary, when using a two-bed approach, the product valve never closes, instead, the intermediate valves VP1 and VP2, open and close so that only the bed that is undergoing the adsorption or pressurization step connects with the tank TP, which connects to the product, constantly increasing its N_2 molar fraction. This is what happens in a real PSA unit, since fictional beds like D1 do not exist in the real world.

Thus, in Model 1, the product stream's composition is equal to the one on TP tank (with known volume and initial composition) while on Model 2 it is equal to the composition in TD2 tank, right above the bed. However, in order to prove the difference in the shape of the curves, a material balance of TP, Equation (13), was performed to modulate the mixture that occurs in this tank, which results in the almost linear shape of the second model's results.

$$y_{iTP_{(t+\Delta t)}} = y_{iTP_{(t)}} + \Delta t \frac{(F_{VP1}y_{iVP1} + F_{VP2}y_{iVP2} - F_{VP}y_{iVP})_{(t)}}{V_{TP}\frac{P}{RT}} \quad (13)$$

This material balance was able to predict TP's molar composition, so the difference in the shape of the curves was explained by the mixture that occurs in TP tank. It is important to refer that this material balance also proved that the volume of the TP tank has a major influence in the simulation's results. In this simulation the volume considered was the default volume of the software for any gas tank, 1 x 10^{-5} m^3, which, with the flowrate considered, results on a passage time of 236 s.

To study the effect of TP's volume, simulations were performed with the volumes of 1 x 10^{-7} m^3 and 1 x 10^{-3} m^3. The results of TP's N_2 molar composition were compared with the first ones, considering a default volume of 1 x 10^{-5} m^3, represented in Figure 18. Using a volume of 1 x 10^{-7} m^3 for TP, the product stream's composition is equal to TOP1/TOP2, meaning that TP's effect is negligible. On the contrary, using a volume of 1 x 10^{-3} m^3, the product's purity decreases.

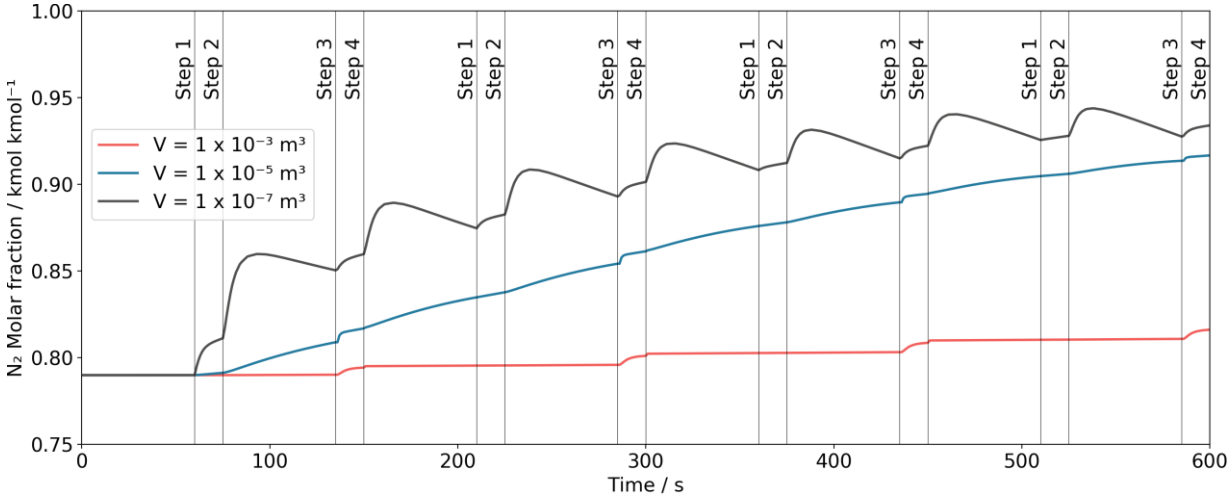


Figure 18 - Effect of TP's volume on the product's N2 molar composition.

Finally, a material balance considering the inlets and outlets of Model 1 was also considered, following Equation (12). It was concluded that the amount of each component on the inlet subtracted by the amount of that component in the outlets, corresponded to the adsorbed amount (solid loading) on one bed subtracted by the desorbed amount on the other bed. A similar material balance was not conclusive using the second model's results since there is no solid loading information on the Gas Interaction block.

After the study and deep understanding of these models, it was concluded that both of them reach the same average purity and take the same number of cycles to reach a cyclic steady state. Even though, Model 2 allows a faster simulation, since the software only needs to perform half the calculations, Model 1 presents a better description of reality and the material balances estimated were proved accurate for this model. Therefore Mode 1 should, preferably, be used for the next simulations.

4.4. Two simulation modes

As explained in Chapter 3, Aspen Adsorption provides two different simulation modes for the simulation of cyclic processes: Gas Dynamic and Gas CSS mode (gCSS). In this Section, the case study was simulated in the different simulation modes and its results were compared. The simulation flowsheets for Model 1 of the Section 4.3, using dynamic (left) and gCSS (right) modes, are presented in Figure 19.

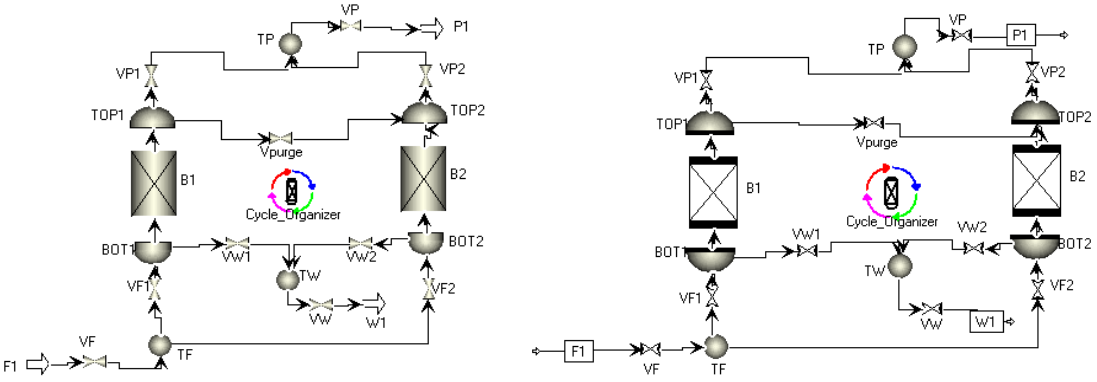


Figure 19 - Simulation flowsheets of a Dynamic and gCSS simulation.

The Extended Langmuir isotherm used in the Dynamic simulations was available in both simulation modes. Using the same specifications and manipulated variables in the cycle organizer, the flowrates' variation was equal in both models even though initial values were not provided in the gCSS simulation mode, since there is not a specific block for the Feed and Product. This only occurs because both pressure values and CV values for the valves were equally specified in both modes, thus, the software adjusted the flowrates in the same manner.

When analyzing the results for the same case simulated in both simulation modes, it was possible to confirm that they converged to different values. This difference may be explained by the distinct discretization methods used: in the dynamic simulation mode a Central Differencing Scheme was used and, in the gCSS simulation a Central Finite Differences method was chosen. In the solver options, step sizes and solver methods were adjusted, in an attempt to minimize the difference between the curves and the best results, Figure 20, were obtained with Implicit Euler, considering a minimum step size of 0.1 and a maximum step size of 1.

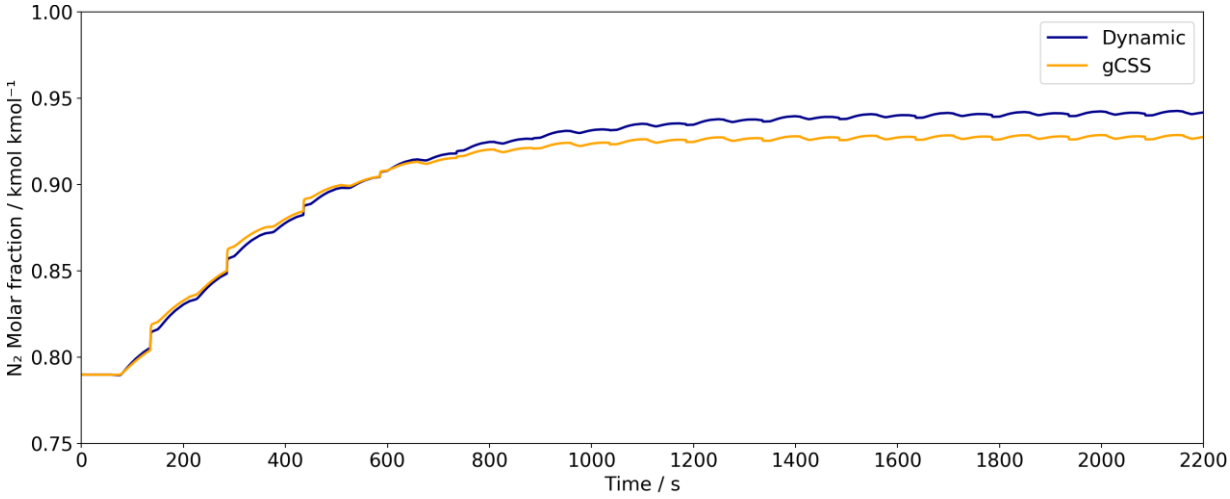


Figure 20 - N_2 molar fraction in P1 in a Dynamic and gCSS simulation.

Finally, the main feature of the gCSS simulation mode was tested: the direct determination of the cyclic steady state before running a dynamic simulation along time. Activating the Cyclic Steady State mode, the software's ability to perform complete discretization of time and space was used and a steady state simulation was executed. The outputs from this simulation, instead of a plot with the variables varying along time, were a list of variables such as temperature, pressure and molar compositions that the system is expected to attain at the Cyclic Steady State. These values can be used afterwards as initial conditions to run a dynamic simulation along time.

It was shown that with or without cyclic steady state determination, the gCSS simulation converges to the same value, slightly below the Dynamic simulation mode's results. The direct determination of the cyclic steady state conditions, possible in the gCSS simulation mode, is a useful feature since it may increase convergence in complex cases. In highly nonlinear problems, starting a simulation with initial values closer to the ones that the system is expected to converge, can make a significant difference. However, for the purpose of comparing both simulation mode's performance, this feature was not considered relevant since it was more important to compare how the system evolved from the same initial conditions in both simulation modes, as illustrated in Figure 20.

5 Validation of Aspen Adsorption's results

The purpose of this chapter is to compare the results obtained from Aspen Adsorption software with experimental and modelling results from published works, chosen according to the criteria detailed in Section 2.3.

Two case studies were considered. The first case study consists in simulating the breakthrough curve presented by Jee et al. [16], where a two-layered bed (activated carbon and zeolite 5A) is used for separating H_2 from a ternary mixture ($H_2/CH_4/CO$). The second case study simulates the PSA operation presented in Yang et al. [17] for the separation of H_2 from a H_2/CH_4 mixture, using Zeolite 5A.

The work developed in this chapter is divided in three sections: Section 5.1 and Section 5.2 present the results of the first and second case study, respectively; Section 5.3 delves into the simulation of the second case study, at industrial scale.

5.1 Analysis of a breakthrough curve

The duration of the adsorption step is usually the starting point for the study of a PSA process. The case study considered for this section consists in a layered bed, packed with activated carbon (type PCB, Calgon Co.) and zeolite 5A (Grace & Davison Co.) for H_2 separation from a ternary mixture ($H_2/CH_4/CO$) (Jee et al., 2001).

The adsorption dynamics of this mixture were simulated using Aspen Adsorption with Dynamic simulation mode, since gCSS mode is only used to simulate cyclic processes. The simulation flowsheet for a breakthrough curve experiment consists of a Gas_Bed connected with a Feed block and a Product block.

The main assumptions for this case, described in [16], were: 1) the gas behaves as an ideal gas mixture; 2) the radial concentration and temperature gradients are negligible (1D); 3) it is a non-isothermal process, with no conduction and considered non-adiabatic; 4) the flow pattern is described by the axially dispersed plug-flow model; 5) the mass transfer rate is represented by a linear driving force (LDF) model and 6) the Ergun equation is applied for the pressure drop along the bed.

Finally, according to the study of Jee et al. [16], the adsorption equilibrium was predicted by the Extended Langmuir-Freundlich model, with dependency of temperature and pressure. Using the gCSS mode, this equation is available in Aspen Adsorption with the name of Loading Ratio Correlation 3 (LRC3). However, in Dynamic mode, this isotherm is not available, thus the Langmuir-Freundlich isotherm with pressure and temperature dependency was used, and its parameters were adjusted, considering a range of temperatures and pressures suited

for the system. The new isotherm parameters were estimated using the least squares method and the coefficient of determination (R^2) obtained was higher than 0.99 for all components (Appendix C).

The specifications of the bed were provided in [16] from its geometry to its adsorbent properties (listed in Appendix D), thermal properties, isotherm parameters, axial dispersion coefficients, heats of adsorption and mass transfer coefficients. The feed was at 10 atm and 298.15 K with a molar composition of 60% H_2, 30% CH_4 and 10% CO and the flowrate considered was 9.1 LSTP/min, which corresponds to a molar flowrate of 6.3 x 10^{-6} kmol/s (considering 1 atm and 293.15 K). The discretization method used in Aspen Adsorption was the Upwind Differencing Scheme.

For the breakthrough curve simulation, similarly to what was presented in [16], the bed was initially filled with H_2. The breakthrough curve obtained from the simulation was compared with the experimental results presented in the paper of Jee et al. (2001) and are depicted in Figure 21.

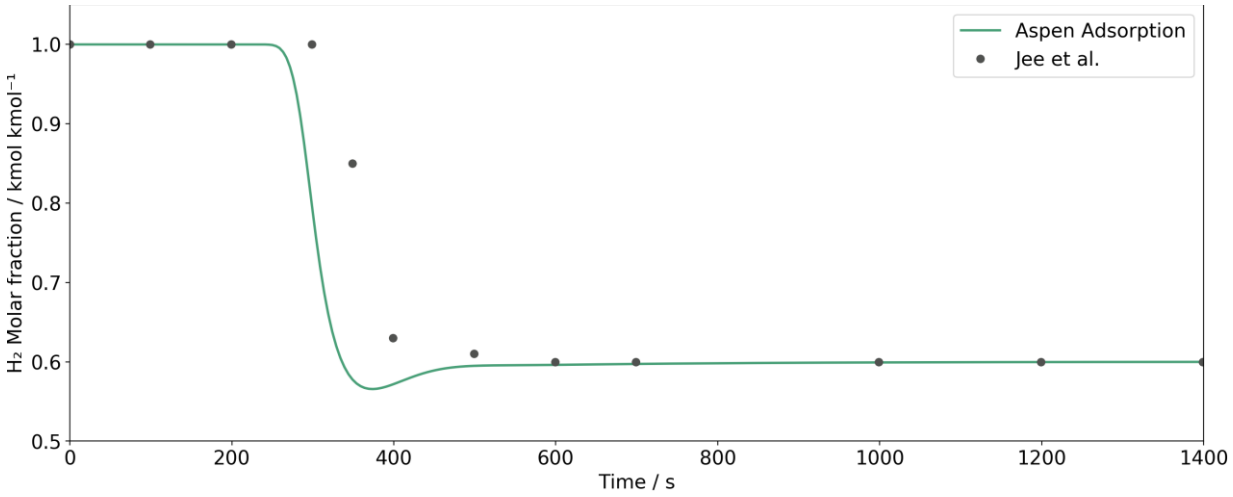


Figure 21 - Breakthrough curve obtained in Aspen Adsorption and in Jee et al.

The maximum performance of adsorption is guaranteed for about 260 s according to the Aspen Adsorption simulation and for about 300 s according to from the paper of Jee et al. [16]. The differences observed can be due to the fact that different isotherms were considered, the Loading Ratio Correlation in [16] and the Langmuir-Freundlich with adjusted parameters in Aspen Adsorption. Also noticeable is a reduction of the molar fraction of H_2 in the outlet, before stabilizing to a composition equal to the feed. This phenomenon is explained by the roll-up of one of the adsorbed components. Since one of them was more strongly adsorbed (CO) and retained within the pores, the other (CH_4) increased its concentration in the bulk phase, leading to a higher concentration than that of the inlet during a few seconds.

5.2 Analysis of a PSA unit for H_2 separation

The case study considered for this section consists in a Pressure Swing Adsorption unit using Zeolite 5A (Davison Chemical Co.) for high-purity H_2 production from a CH_4/H_2 mixture (Yang et al., 1997).

In Aspen Adsorption, as mentioned in the previous chapters, two simulation modes allow the simulation of adsorption cyclic processes. For the first simulations of this case, the gCSS simulation mode was chosen and the simulation flowsheet was built based on Model 1, illustrated in Figure 13, with two similar adsorption beds. The main assumptions of this model, described in [17] were: 1) the flow pattern is described by the axially dispersed plug-flow model; 2) it is a non-isothermal and non-adiabatic problem, with no conduction; 3) the mass transfer rate is represented by a linear driving force (LDF) model; 4) the gas behaves as an ideal gas mixture; 5) the radial concentration and temperature gradients are negligible (1D) and 6) the Ergun equation is applied for the pressure drop along the bed.

The adsorption equilibrium was also described by the Extended Langmuir-Freundlich model, with dependency of pressure and temperature, in gCSS mode named as Loading Ratio Correlation 3. The geometry of the bed, its adsorbent properties (listed in Appendix D), thermal properties, isotherm parameters, axial dispersion coefficients, heats of adsorption and mass transfer coefficients were provided in [17]. The discretization method used in this simulation was the 2nd order Central Finite Difference.

The PSA cycle of each bed consists of the six following steps: 1) feed pressurization (30 s), 2) high-pressure adsorption (180 s), 3) depressurizing pressure equalization (40 s), 4) countercurrent depressurization/blowdown (30 s), 5) purge (180 s) and 6) pressurizing pressure equalization (40 s). Bed 1 is always two steps ahead of Bed 2 during the cycle. During pressure equalization steps, all valves are closed except the purge valve, which connects the two bed.

The feed stream was specified with 11 atm and 298.15 K (one of the scenarios presented in [17]) with a molar composition of 30% CH_4 and 70% H_2. Since, the goal of this study was to produce high-purity H_2, the typical operating parameters of the PSA, such as adsorption pressure, Purge to Feed ratio (P/F) and the step times have a major influence in the results. In order to replicate the paper's conditions, the P/F ratio should be 0.1 and the flowrate should have a constant value of 2 L/min at the feed's inlet conditions.

When moving from the tutorials to the simulation of a published work on PSA, some complexity was added, particularly in the flowrate control. Tutorials and examples were explicit in terms of the valve's CV used, while published papers indicate some of the flowrates considered without detailing the valve's specifications for each step of the cycle.

A deeper study was then conducted, to understand how the flowrates used in Yang et al. [17] could be reproduced in a simulation. Considering a constant feed flowrate during pressurization and adsorption, as mentioned in [17], the pressure increased to values higher than the desired ones (45 bar). Then, in order to keep the pressure at the desired value, the purge and product CVs were adjusted, however, the purity obtained varied during each cycle (70%-90%). Finally, with the feed flowrate at the constant value designated in [17], the product valve was left completely open, in order to allow the software to calculate its flowrate. With this option, once again, low purities around 70% were attained. (Appendix E)

Then, it was concluded that if the flowrate condition was relaxed, higher purities could be achieved, and the pressure could be held in the desired value during adsorption. Following this consideration, the feed flowrate was held constant only during pressurization, while during adsorption, VF valve was left completely open to allow the software to infer the appropriate feed flowrate, in order to maintain the adsorption pressure as well as the desired purge and product flowrates that allow high purity. During pressure equalization, the feed flowrate is null, since only the purge valve, VPurge, is open. Therefore, Yang et al. [17] conditions were not exactly reproduced, since the feed flowrate would vary during the PSA experiment. An alternative to this method would be to change the step times of the cycle.

5.2.1 Flowrate control

A strategy was then developed for the flowrates control during the PSA cycle, which can be applicable to all PSA cases, simulated in this software package.

The first step is to estimate the adequate feed flowrate during pressurization. It can be calculated considering ideal gas behavior for the initial and final state of pressurization and the amount adsorbed in that pressure range (calculated from the isotherm), divided by the step's duration.

The second step is to calculate the feed and waste valves' CV for pressurization and depressurization steps, where product (VP1 or VP2) and purge valves are closed. As mentioned in Chapter 3, in linear valves, the CV can be expressed considering the ratio between the flowrate and the pressure drop through the valve. However, in steps when this pressure drop through a valve is not constant, such as pressurization and depressurization, the CV of the valves can be derived using the bed's conditions and the step's duration from the ideal gas equation, resulting in Equation (14). (Appendix F)

$$CV = \frac{V_B}{R\,T_B t_{step}} \ln\left(\frac{P_{B\,start} - P_{Ext}}{P_{B\,end} - P_{Ext}}\right) \quad (14)$$

Here, V_B is the volume of the bed, T_B the temperature of the bed, R the ideal gas constant, t_{step} is the step's duration, $P_{B\ start}$ and $P_{B\ end}$ the pressure of the bed at the start and end of the step, $P_{Ext\ start}$ and $P_{Ext\ end}$ the external pressure at the start and end of the step.

The third step is to calculate the purge and product valves' CV, for the adsorption/purge steps. These can be calculated through the ratio between the desired flowrate and the ΔP through the valve, which assumes an approximately constant value. Knowing the desired Purge to Feed ratio, the purge flowrate and CV can be calculated. During the adsorption step, VF, VPurge and VP valves are open, thus, the flowrate through VP should be equal to the difference between the feed and purge flowrates. After calculating this flowrate, VP's CV is also estimated. As mentioned, during adsorption/purge, the feed valve, VF, is left completely open to allow the software to calculate, in each second, the appropriate value of the feed flowrate. During pressure equalization steps, the same CV for the purge valve was considered.

The fourth step, is to run a first simulation in order to confirm that the estimated feed flowrate in the first step, is close to the one calculated by the software with the given CV from Equation (14) to achieve pressurization in the step's duration. If verifiable, the estimated feed flowrate can then be held constant in the cycle organizer during pressurization steps and the CVs can be adjusted in order to optimize the results. The final run is executed with all the referred valve's configuration. For this case study, the specifications are listed in Table 7.

Table 7 - Specification of the PSA cycle for the H_2 separation

	Press. B1 **Blowdown B2**	**Adsorption B1** **Purge B2**	**Pressure equalization**	**Press. B2** **Blowdown B1**	**Adsorption B2** **Purge B1**	**Pressure equalization**
VF	3 (F =2.2 x 10^{-5} kmol/s)	1	1	3 (F =2.2 x 10^{-5} kmol/s)	1	1
VF1	1	1	0	0	0	0
VF2	0	0	0	1	1	0
VPurge	0	2 (Cv=3.0 x 10^{-8} kmol/s/bar)	2 (Cv=3.0 x 10^{-8} kmol/s/bar)	0	2 (Cv=3.0 x 10^{-8} kmol/s/bar)	2 (Cv=3.0 x 10^{-8} kmol/s/bar)
VP	2 (Cv=2.7 x 10^{-7} kmol/s/bar)	2 (Cv=2.7 x 10^{-7} kmol/s/bar)	2 (Cv=2.7 x 10^{-7} kmol/s/bar)	2 (Cv=2.7 x 10^{-7} kmol/s/bar)	2 (Cv=2.7 x 10^{-7} kmol/s/bar)	2 (Cv=2.7 x 10^{-7} kmol/s/bar)
VP1	0	1	0	0	0	0
VP2	0	0	0	0	1	0
VW	2 (Cv=1.0 x 10^{-5} kmol/s/bar)	2 (Cv=1.0 x 10^{-5} kmol/s/bar)	2 (Cv=1.0 x 10^{-5} kmol/s/bar)	2 (Cv=1.0 x 10^{-5} kmol/s/bar)	2 (Cv=1.0 x 10^{-5} kmol/s/bar)	2 (Cv=1.0 x 10^{-5} kmol/s/bar)
VW1	0	0	0	1	1	0
VW2	1	1	0	0	0	0

Using these specifications in the cycle organizer, the flowrate obtained for the purge was 5 x 10^{-7} kmol/s, for the product 2.7 x 10^{-6} kmol/s and for the feed, the flowrate had a constant value of 2.2 x 10^{-5} kmol/s during pressurization and varied between that value and 5 x 10^{-6} kmol/s during adsorption. The P/F ratio tended to a plateau of 0.1 during adsorption, as desired.

5.2.2 Purity and Recovery

The specifications in the cycle organizer described before were used to keep the P/F ratio similar to the one used in the work of Yang et al. [17] as well as the step times and the adsorption pressure. The simulation was run during 10 cycles. The molar fractions of the components in the product stream are represented in Figure 22 and the pressure profile is represented in Figure 23.

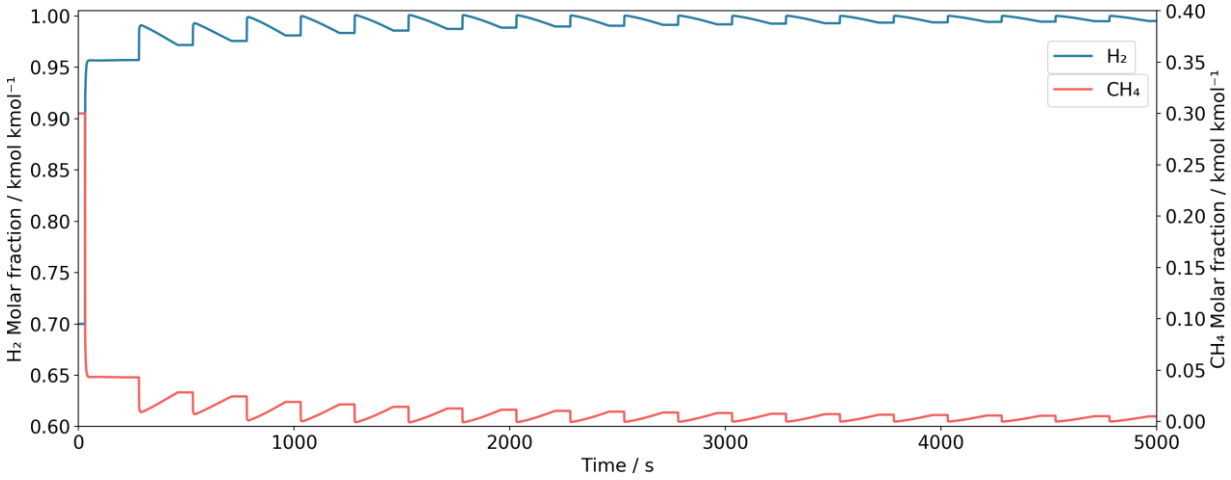


Figure 22 - Molar fractions of the components in the product stream, during 10 cycles.

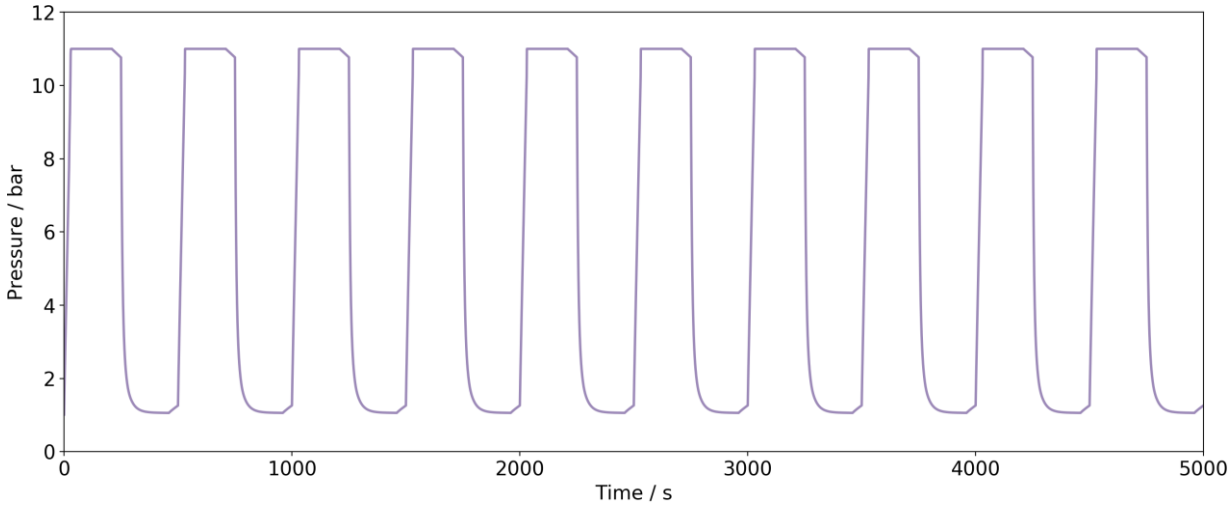


Figure 23 - Pressure inside Bed 1 during 10 cycles.

In order to monitor PSA separation units, two important parameters are commonly calculated, purity, Pur_{H2}, (Equation 15) and recovery, Rec_{H2}, (Equation 16). While purity represents the proportion of the target component in the product stream (in this case H_2), recovery relates the amount of target component (H_2) in the product with the amount of the target component (H_2) fed to the adsorption bed.

$$Pur_{H2} = \frac{\int_0^{t_{ads}} y_{H_2} F_{P1} dt}{\sum_{i=1}^{N} \int_0^{t_{ads}} y_i F_{P1} dt} \quad (15)$$

$$Rec_{H2} = \frac{\int_0^{t_{ads}} y_{H_2} F_{P1} dt}{\int_0^{t_{ads}} y_{H_2} F_{F1} dt + \int_0^{t_{press}} y_{H_2} F_{F1} dt} \quad (16)$$

Here, N stands for the number of components, t_{ads} for the adsorption time and t_{press} for the pressurization time.

A Dynamic simulation was also performed, considering the same adjustment of the isotherm mentioned in Section 5.1 (Appendix C), in order to compare the gCSS and Dynamic results for this separation, represented in Figure 24.

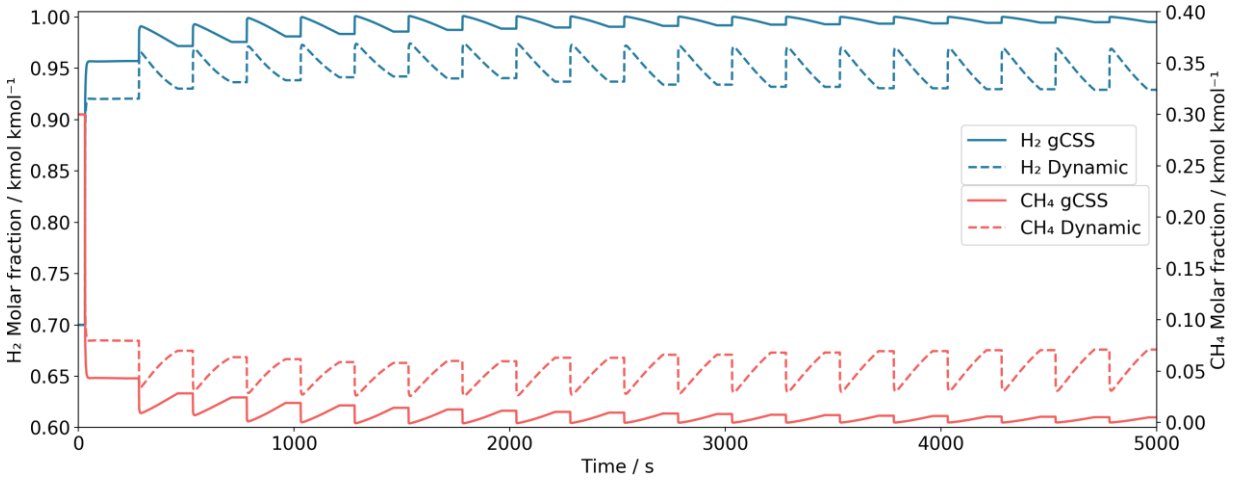


Figure 24 - Comparison of the molar fractions of components in the product stream for in the gCSS and Dynamic simulation, during 10 cycles.

The purity and recovery were estimated with the results of the last cycle (4500 s - 5000 s) and were compared with the results from the study of Yang et al. [17] for the same conditions (Table 8).

Table 8 - Purity and recovery values from Aspen Adsorption simulations compared with the values in Yang et al.

	Purity	Recovery
Yang et al. [17]	99.8%	75%
gCSS simulation	99.6%	68%
Dynamic simulation	94.9%	67%

The gCSS simulation mode provided the best results, especially in terms of purity. However, the recovery value calculated based on the simulation's results presented a relative error of 9% when compared to the paper's results. This error was due to the fact that in Aspen Adsorption's simulations the feed flowrate was not kept constant during adsorption steps and had a higher value than that referred in [17] during pressurization.

5.2.3 Axial profiles

The variation of H_2 molar fraction along the bed length at the end of the adsorption step of cycle 10 was also plotted. Yang et al. [17] predicted these axial profiles considering an adsorption pressure of 11 atm. These predictions were compared with the results extracted from the gCSS simulation in Aspen Adsorption and are represented in Figure 25, with error bars representing 3% of error of the values predicted by Yang et al. [17].

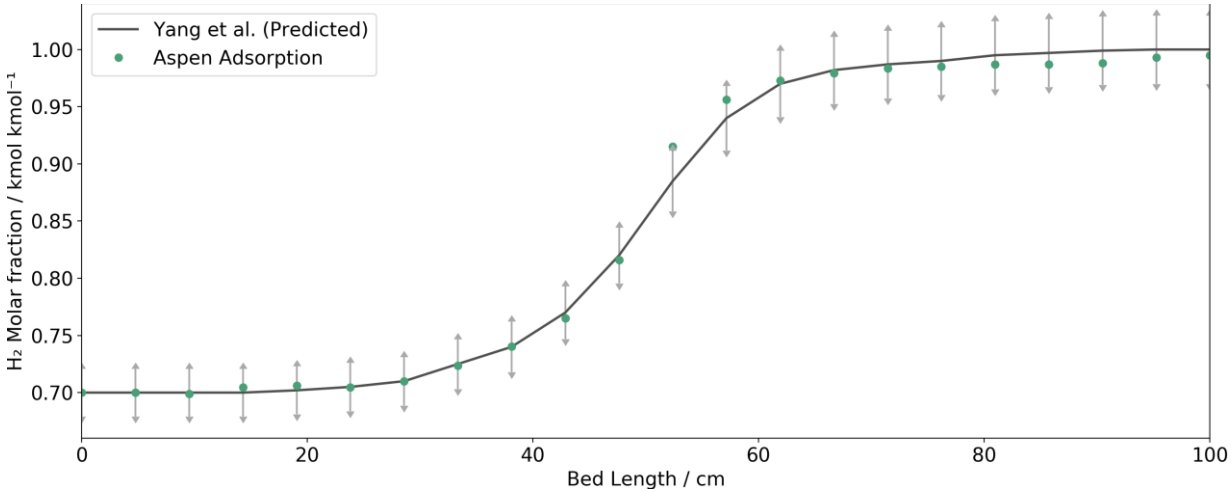


Figure 25 - H_2 molar fraction along the bed length at the end of the adsorption step of cycle 10.

A similar study was performed, but this time for the CH_4 solid loading. The predicted profiles from [17] at the end of the adsorption step were compared with Aspen Adsorption gCSS simulation's results, at 11 atm, and are represented in Figure 26. The error bars represented correspond to the constant value of 3% of error of the of first value predicted by Yang et al. [17].

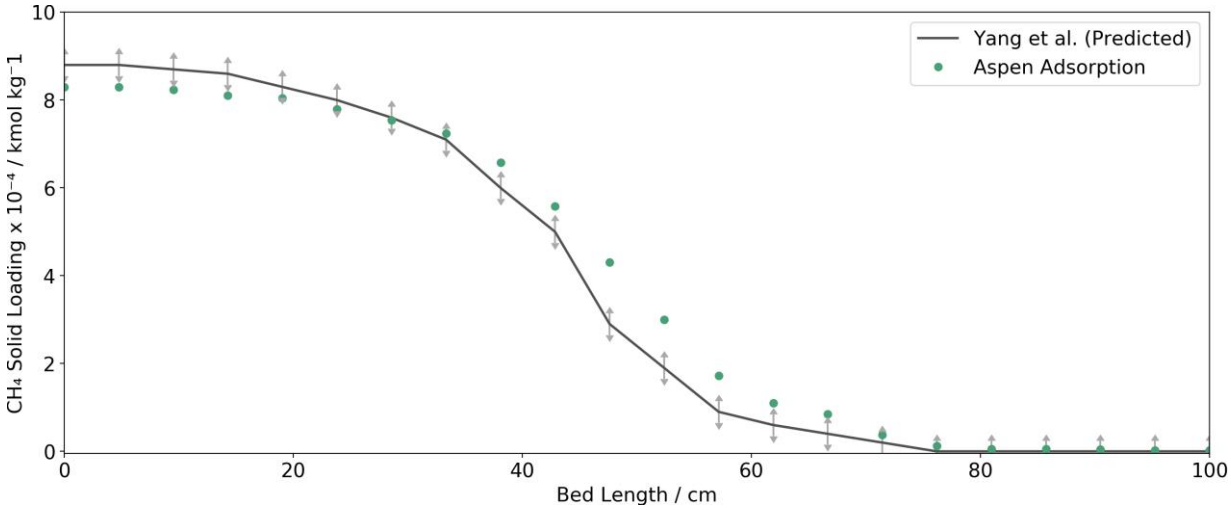


Figure 26 - CH_4 solid loading along the bed length at the end of the adsorption step of cycle 10.

Aspen Adsorption's axial profiles for both H_2 molar fraction and CH_4 solid loading were considered to be very close to the predicted values from Yang et al. [17], being that most of the results from Aspen Adsorption are comprehended within the 3% error bars considered.

5.3 Simulation of a PSA Unit for H_2 Separation at Industrial Scale

A simulation of a PSA unit for H_2 separation at industrial scale was performed, supported on the case study described in Section 5.2. The adsorption bed, described in [17], had a height of 1 m and a diameter of 4.4 cm, the bed porosity was 0.316, meaning that the effective volume of the bed was 4.8 x 10^{-4} m^3. The feed flowrate during adsorption was 0.081 kg/h and the product flowrate, containing 99.6% pure H_2, was 0.019 kg/h. During pressurization, the feed flowrate was 2.2 x 10^{-5} kmol/s, which corresponds to 0.49 kg/h.

The industrial scale dimensions considered for the beds were a height of 10 m, a diameter of 4 m (based on [18]), with the same bed porosity as the initial case, which results in an effective volume of 39.7 m^3. Since the volume increase of the bed was around 80 000 times, the volume of the tank voids should be increased in the same proportion. In the lab scale case, the tanks had a volume of 1 x 10^{-5} m^3 and should be scaled-up to 0.8 m^3. The feed flowrate during adsorption increased to 4040 kg/h and the product flowrate, 99.6% pure H_2, increased to 1080 kg/h. The pressurization of the bed (considering the same step duration of [17]) took a feed flowrate of 1.8 kmol/s, which corresponds to 40176 kg/h.

The strategy used for the definition of the new valve's CV was the same used for the lab scale case, previously described in Section 5.2.1. Therefore, the increase in the valves' CV was in the same proportion as the increase of the volumes, meaning the space time, defined as the ratio between the volume of the bed and the feed flowrate, was kept in the same order of magnitude.

It is also important to consider the Ergun's pressure drop, which can be affected if the same particle size is considered. The superficial velocities should be calculated for the case study based on [17] and for the industrial scale case, and the Ergun's pressure drop compared. In cases where the pressure-drop changes with industrial scale dimensions, the particle size should be adjusted. In this case, using the same particle size as that used in the paper of Yang et al. [17], considering a superficial velocity equal to 3.4 x 10^{-3} m/s, and with the specified bed volume, a pressure drop of 78.8 bar was obtained (7 times larger than that from the bed at the lab scale).

Finally, dimensionless parameters such as the Peclet number should also be analyzed. In this case, the Peclet number for axial dispersion was calculated by Equation (17). It measures the relative contribution of convective flux to diffusive flux [19].

$$Pe = \frac{d_p v_g}{D_{Li}} \quad (17)$$

Here, d_p is the diameter of the particle, v_g is the superficial velocity and D_{Li} is the axial dispersion. Both in the lab scale and in the industrial scale cases, the Peclet number should be similar. This is generally achieved by adjusting the particle size. Using the same particle size as that used in the paper of Yang et al. [17], the Peclet number for the industrial scale case was 0.3 (3.4 times smaller than that from the lab scale).

Table 8 lists the calculated parameters for both cases and the particle size considered in order to keep Ergun's pressure drop and the Peclet number in the same value for the lab scale and the industrial scale case.

Table 9 - Parameters calculated for the lab scale and industrial scale cases

	τ adsorption (s)	**τ pressurization (s)**	**v_g (m/s)**	**rp (m)**	**ΔP (bar)**	**Pe**
Lab scale	59.8	9.82	5.2 x 10^{-3}	1.57 x 10^{-3}	11.2	1.11
Industrial scale	85.7	9.92	3.4 x 10^{-3}	4.02 x 10^{-3}	11.2	1.02

The feed flowrate for pressurization in the industrial scale case was re-adjusted when the particle size was changed. Originally, it was 1.74 kmol/s, with a particle radius of 1.57 mm, and had to be increased to 1.8 kmol/s, considering a particle radius of 4.01 mm.

The molar fractions of the components in P1 for the industrial scale and lab scale case are represented in Figure 27 and the pressure variation in Bed 1 for both cases in Figure 28.

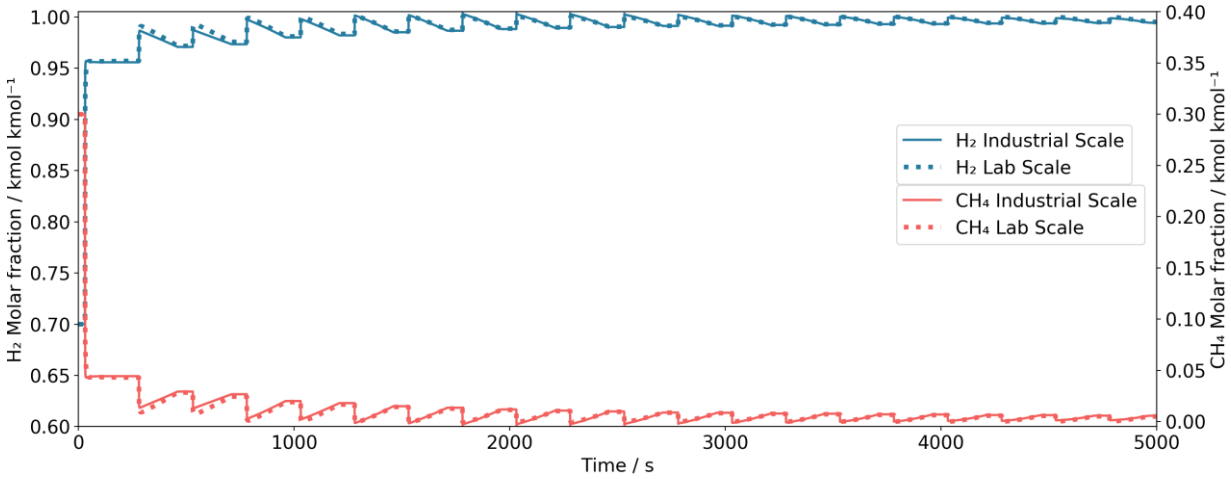


Figure 27 - Molar fractions of the components in the product stream for the industrial and lab scale cases during 10 cycles.

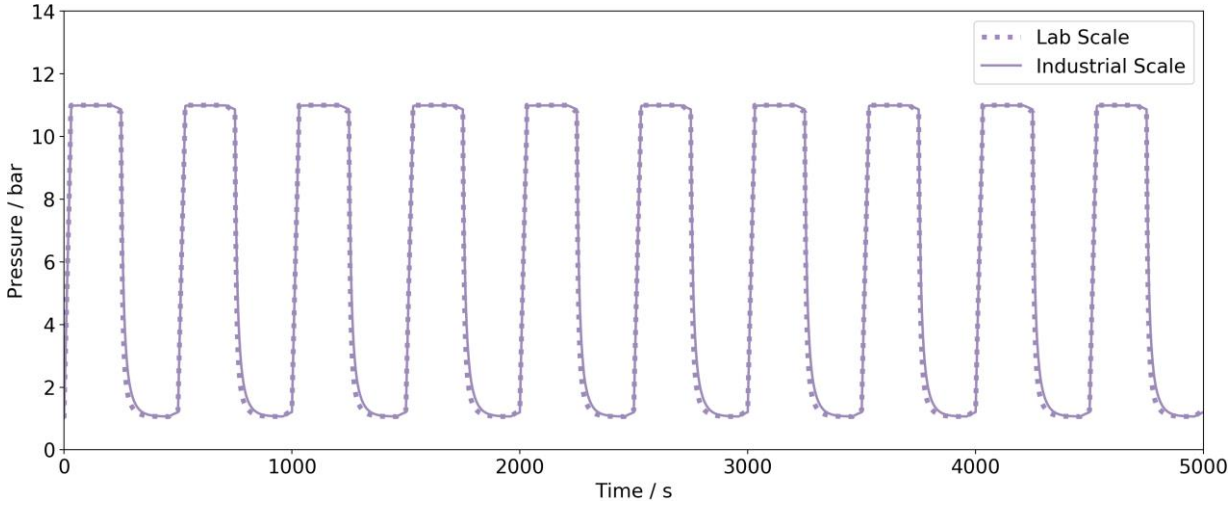


Figure 28 - Pressure variation in Bed 1 along the 10 cycles for industrial and lab scale cases during 10 cycles.

The purity obtained for both the industrial scale and lab scale case were similar (higher than 99%), with a volume and a flowrate increase in the same order of magnitude, around 80 000 times.

While performing the study of the industrial scale simulations, another detail was found. When the fixed feed flowrate specified for the pressurization is not enough to fully pressurize the bed in the step's duration, the software rises the bed's pressure in the first seconds of the adsorption step, since the feed valve is completely open. If not carefully analyzed, it may seem that the given flowrate was enough for the desired pressurization during the step's duration, even though it was not.

Figure 29 illustrates this occurrence with a feed flowrate of 1.5 kmol/s in the industrial scale simulation, which only allows pressurization up to 8 bar in the step's duration. Once again, the importance of carefully analyzing the results from the software is proved.

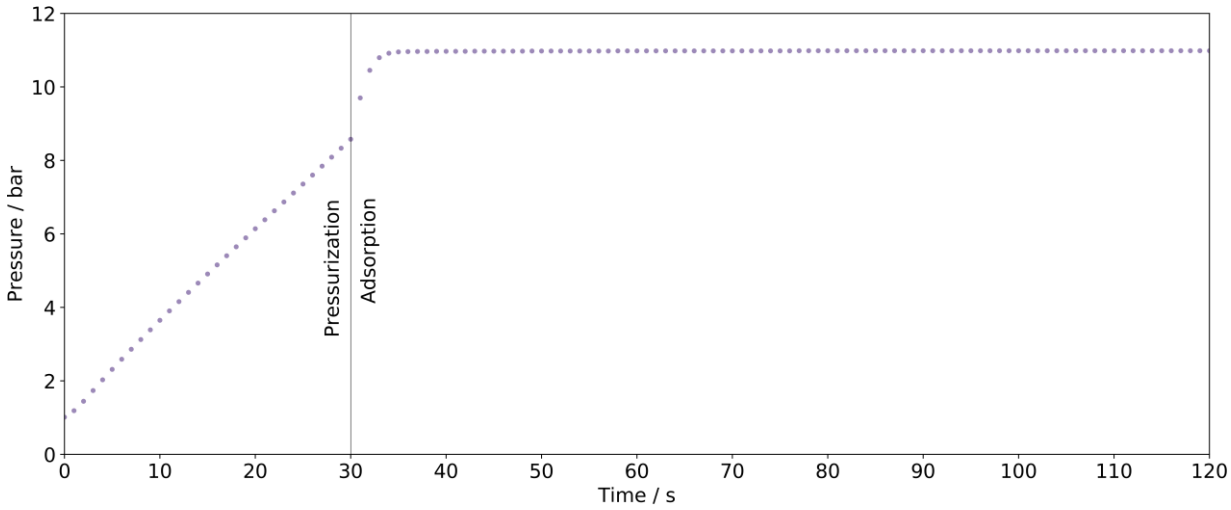


Figure 29 - Pressure variation in Bed 1 in the first 100 seconds of the simulation, with a feed flowrate unable to fully pressurize the bed.

It is worth mentioning that typically, an industrial scale PSA unit is far more complex than the one developed in this chapter, including multiple beds and far more complex cycles. Usually, the scale-up of those units starts with the definition of a target flowrate, and in order to prevent fluidization or to separate multiple components from a mixture, several industrial-scale beds are projected.

The goal of this work was mainly to study the considerations to transform a laboratory scale two-bed PSA into and industrial scale one, acknowledging that it was a simplification of most industrial PSA units. However, in the future, different strategies can be explored for the simulation of industrial PSA units with multiple beds, using Aspen Adsorption.

6 Conclusions

Aspen Adsorption is a flowsheet simulator for the analysis, design, simulation and optimization of industrial and laboratory scale adsorption processes. After a literature review it was concluded that it is, indeed, widely used for several processes such as ion exchange, liquid phase adsorption and gas phase adsorption with adsorption only or with reactive gas adsorption processes.

A deeper analysis was conducted to understand how the software works, from its necessary inputs, governing equations and available numerical methods to its possible outputs. A flow diagram was constructed to summarize the main steps in every Aspen Adsorption simulation.

After that, PSA simulations were studied in detail. Firstly, some assumptions of the software were analyzed by simulating adsorption and desorption steps on a single bed, then two models for PSA units were tested and its results compared and finally, the two simulation modes provided by Aspen Adsorption for gas cyclic separations were also examined. It was concluded that both models for PSA separations achieve the same average purity and the same number of cycles to reach the cyclic steady state. However, the designated Model 1, with two adsorption beds, was a closer representation of reality, although the use of a gas interaction block instead of the second bed, as presented in Model 2, allows faster simulations since it requires less numerical capacity.

Hydrogen separations in PSA units were simulated using this software and the results obtained were in fair good agreement with the results from published papers on the same separations. In fact, the gCSS simulation mode proved to have closer results to the experimental and predicted values from literature in these simulations. A simulation of an industrial scale two-bed PSA was also performed, and its results were considered suitable.

Aspen Adsorption is definitely a complete and powerful tool for the design and optimization of adsorption processes, including PSA units. It allows the use of Aspen Properties database, which represents an advantage of its utilization. However, some challenges were noticed while using the software, sometimes predicting non-realistic results, without retrieving warnings or error messages for them, which increases the responsibility of the user on its interpretation. Examples include the output of compositions of a stream when its flowrate is null and the reverse flow in valves caused by numerical errors. It is recommended that all outputs are carefully analyzed for a better understanding of the software and a correct interpretation of the results. Lastly, the differences between the simulation modes, particularly the isotherm packages available, which led to adjustments in the isotherm parameters, were also considered a challenge in the software's study.

6.1 Accomplished objectives

The main objective of this thesis was the exploration of Aspen Adsorption software capability to simulate PSA processes, to assess the potential of its use within Net4CO2 activities, and to understand its main advantages and disadvantages. PSA units are widely used in industrial processes, including in process routes with relevance for the carbon dioxide circular economy and for energy systems which are likely to be part of the new energy paradigm, such as synthetic fuel and hydrogen production. Therefore, using a tool to simulate these processes is of great relevance to Net4CO2.

For this purpose, an extensive literature review using the PRISMA Methodology was performed to understand the software's acceptance and its main applications; the execution of a set of tutorials to understand how the software works and its main features was also carried out; comparative studies on alternatives to simulate Pressure Swing Adsorption units using Aspen Adsorption were performed; finally, Aspen Adsorption's results were validated with published works, a strategy was developed for the flowrate control and a larger scale PSA unit for H_2 separation was simulated in Aspen Adsorption. In conclusion, the objectives of this work were considered accomplished.

6.2 Limitations and Future Work

The main limitations of this work were based on the complexity of the software and its several critical details. The study and understanding of these details and how the software modulates the physical phenomenon of adsorption, which was considered essential for the software understanding, limited a further exploration of more complex PSA units.

Future work incudes simulation of industrial scale Pressure Swing Adsorption units for H_2 separation in scenarios with multiple bed and more complex cycles and further exploration of the subroutines that allow the introduction of user-defined isotherms.

6.3 Final assessment

The development of this work was, indeed, very enrichening from a personal level since it enabled the exploration of a new software and the deeper study of adsorption processes, particularly Pressure Swing Adsorption. With this work, one was able to bring some expertise to Net4CO2 regarding Aspen Adsorption and its capacity to simulate PSA units, which may have a significant impact in the study of scenarios including adsorption and PSA processes in the future.

7 References

[1] NASA. *Climate Change: Vital Signs of the Planet*. Available at: https://climate.nasa.gov/ (Accessed 10 Feb. 2020)

[2] IEA. IEA – International Energy Agency. Available at: https://www.iea.org/ (Accessed 10 Feb. 2020)

[3] Yáñez, M., Relvas, F., Ortiz, A., Gorri, D., Mendes, A., Ortiz, I. PSA Purification of waste hydrogen from ammonia plants to fuel cell grade. *Separation and Purification Technology*, 240. (2019)

[4] Pratiwi, V., Juwari, J., Handogo, R. Simulation of Hydrogen Purification using Two Bed System Pressure Swing Adsorption. *IPTEK Journal of Proceedings Series*, 14. (2017)

[5] Abdeljaoued, A., Relvas, F., Mendes, A., Chahbani, M.H. Simulation and experimental results of a PSA process for production of hydrogen used in fuel cells. *Journal of Environmental Chemical Engineering*, 6. (2017)

[6] Silva, B., Solomon, I., Ribeiro, A.M., Chang, J., Loureiro, J.M., Rodrigues, A.E. H2 purification by Pressure Swing Adsorption using CuBTC. *Separation and Purification Technology*, 118. (2013)

[7] Asgari, M., Anisi, H., Mohammadi, H., Sadighi, S. Designing a commercial scale pressure swing adsorber for hydrogen purification. *Petroleum and Coal,* 56. (2014)

[8] Wood, K., Liu, Y. and Yu, Y. Design, simulation and optimization of adsorptive and chromatographic separations. John Wiley & Sons, 2018.

[9] Medrano, J., Llosa-Tanco, M., Tanaka, D., Gallucci, F. Membranes utilization for biogas upgrading to synthetic natural gas. (2019)

[10] Thomasnet.com. *What Is Pressure Swing Adsorption?* Available at: https://www.thomasnet.com/insights/what-is-pressure-swing-adsorption-/ (Accessed 3 Feb. 2020)

[11] Grande, C. Advances in Pressure Swing Adsorption for Gas Separation. *ISRN Chemical Engineering*. (2012)

[12] Psenterprise.com. *Chemicals & Petrochemicals - Advanced Cyclic Separation Process Modeling Focus*. Available at: https://www.psenterprise.com/sectors/chemicals/separation/adsorption-landing-/ (Accessed 9 June 2020)

[13] Aspen Tech. Aspen Adsim 2004.1, Adsorption Reference Guide, 2005.

[14] Aspen Tech. Introduction to Aspen Adsorption, AspenTech Customer Education Training Manual, 2008.

[15] Prisma-statement.org. *PRISMA*. Available at: http://www.prisma-statement.org/ (Accessed 3 Feb. 2020)

[16] Jee, J.G., Kim, M.B., Lee, C.H. Adsorption Characteristics of Hydrogen Mixtures in a Layered Bed: Binary, Ternary, and Five-Component Mixtures. *Industrial & Engineering Chemistry Research*, 40. (2001)

[17] Yang, J., Lee, C.H., Chang, J.W. Separation of Hydrogen Mixture by a Two-Bed Pressure Swing Adsorption Process Using Zeolite 5A. *Industrial and Engineering Chemistry Research*, 36. (1997)

[18] Ribeiro, A.M., Santos, J., Rodrigues, A.E., Rifflart, S. Syngas Stoichiometric Adjustment for Methanol Production and Co-Capture of Carbon Dioxide by Pressure Swing Adsorption. *Separation Science and Technology - SEPAR SCI TECHNOL,* 47. (2012)

[19] Tien, C. *Adsorption Calculations And Modeling*. Butterworth-Heinemann,1994.

Appendices

Appendix A – PRISMA Methodology

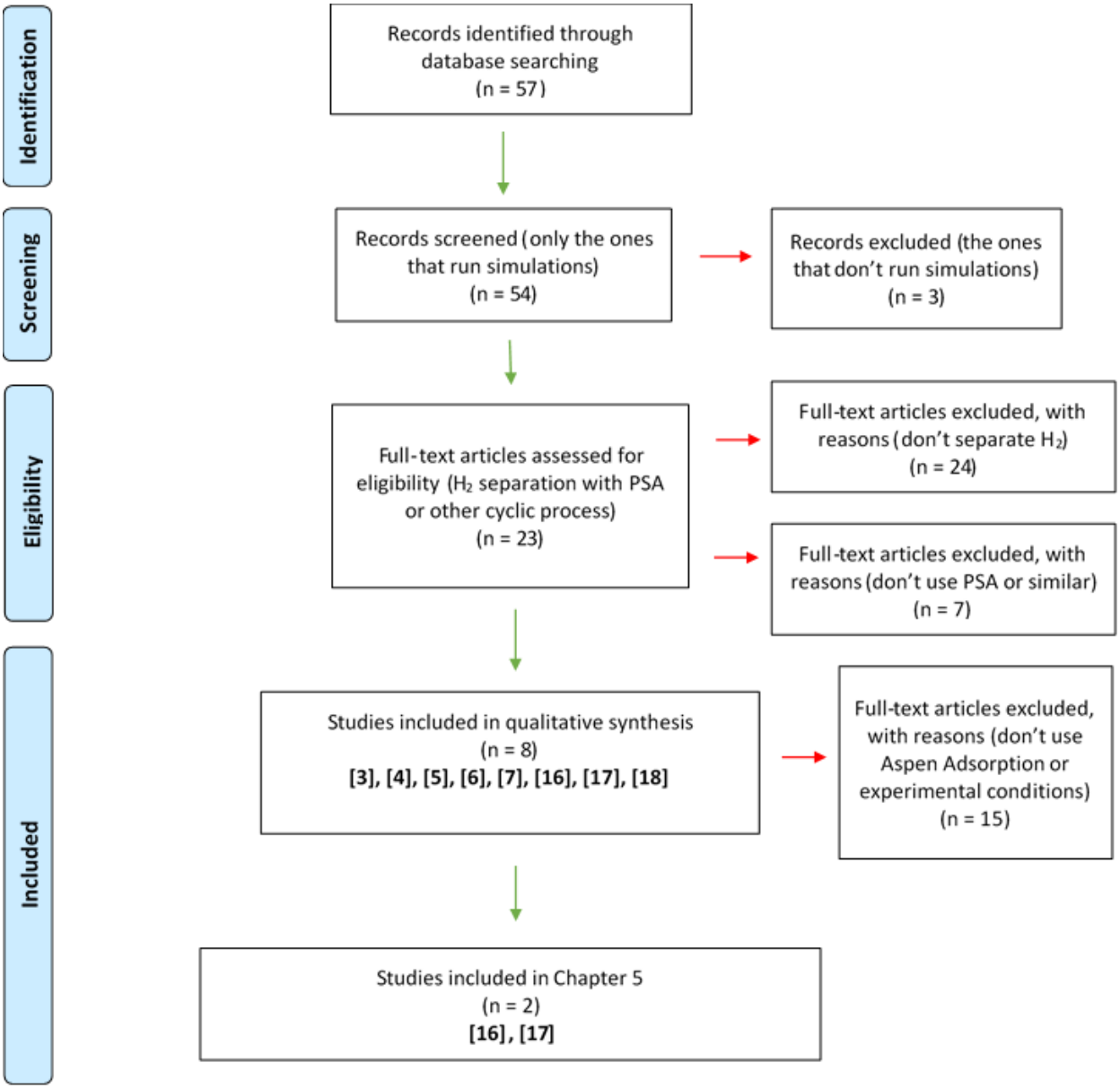


Figure A.1 – PRISMA flow diagram for the literature review.

Appendix B – Numerical methods

1. Example of a discretization method of the Dynamic simulation mode: Upwind Differencing Scheme 1 (UDS1)

UDS 1 is a first-order upwind differencing scheme, based on a first-order Taylor expansion. Its first-order term is given by Equation B.1 and it second-order term is approximated with a second-order accurate central differencing scheme, given by Equation B.2.

$$\frac{\partial \phi_i}{\partial x} = \frac{\phi_i - \phi_{i-1}}{\Delta x} \quad \text{(B.1)}$$

$$\frac{\partial^2 \phi_i}{\partial x^2} = \frac{\phi_{i+1} - 2\,\phi_i + \phi_{i-1}}{\Delta x^2} \quad \text{(B.2)}$$

Where, ϕ is the dependent variable and x is the independent spatial variable.

2. Example of a discretization method of the gCSS simulation mode: Finite Difference Method of nth-order

In the finite difference method, the first-order and second-order partial derivatives are approximated by finite difference formulas derived using Taylor series expansions. The general forms of these equations are given by Equation B.3 (first-order) and Equation B.4 (second-order).

$$\frac{\partial \phi}{\partial x} = \left(\frac{1}{ah}\right) A^{[n]} \phi \quad \text{(B.3)}$$

$$\frac{\partial^2 \phi}{\partial x^2} = \left(\frac{1}{bh}\right) B^{[n]} \phi \quad \text{(B.4)}$$

Where h is the element spacing, $\frac{1}{a}$ and $\frac{1}{b}$ are the multiplying constants, n is the order of approximation and A and B are the differentiation matrixes (the elements of the matrix are the weighting coefficients of nth-order approximations at the n+1 Taylor series points).

Appendix C – Isotherm adjustments (gCCS to Dynamic)

1. Loading Ratio Correlation 3 (gCSS)

$$Q_i = \frac{(IP_{1i} + IP_{2i}T_S)\left(IP_{3i}\exp\left[\frac{IP_{4i}}{T_S}\right]\right)(Py_i)^{IP_{5i}+IP_{6i}/T_S}}{1+\sum_k\left\{\left(IP_{3k}\exp\left[\frac{IP_{4k}}{T_S}\right]\right)(Py_k)^{IP_{5k}+IP_{6k}/T_S}\right\}} \quad \text{(C.1)}$$

2. Langmuir-Freundlich (Dynamic)

$$Q_i = \frac{IP_1 IP_2 P_i^{IP_3}\exp\left(\frac{IP_4}{T_S}\right)}{1+IP_5 P_i^{IP_3}\exp\left(\frac{IP_6}{T_S}\right)} \quad \text{(C.2)}$$

Table C.1 - Parameters used for the Loading Ratio Correlation 3 isotherm, according to Jee et al. (2001) for case study 1

	IP1 (kmol/kg)	IP2 (kmol/kg/K)	IP3 (1/bar)	IP4 (K)	IP5 (-)	IP6 (K)
Activated carbon Layer: CH_4	2.38 x 10^{-2}	-5.61 x 10^{-5}	3.48 x 10^{-3}	1159	1.62	-248.9
Activated carbon Layer: CO	3.38 x 10^{-2}	-9.07 x 10^{-5}	2.31 x 10^{-4}	1751	3.05	-654.4
Activated carbon Layer: H_2	1.69 x 10^{-2}	-2.10 x 10^{-5}	6.25 x 10^{-5}	1229	0.98	43.03
Zeolite Layer: CH_4	5.83 x 10^{-3}	-1.19 x 10^{-5}	6.51 x 10^{-4}	1731	0.82	53.15
Zeolite Layer: CO	1.18 x 10^{-2}	-3.13 x 10^{-5}	2.02 x 10^{-2}	763	3.82	-931.3
Zeolite Layer: H_2	4.31 x 10^{-3}	-1.06 x 10^{-5}	2.52 x 10^{-3}	458	0.98	43.03

Table C.2 – Calculated parameters for the Langmuir-Freundlich isotherm for case study 1

	IP1 (kmol/kg)	IP2 (1/bar)	IP3 (-)	IP4 (K)	IP5 (1/bar)	IP6 (K)
Activated carbon Layer: CH_4	2.29 x 10^{-3}	4.58 x 10^{-3}	0.62	1351.6	8.76 x10^{-9}	0.999
Activated carbon Layer: CO	1.33 x 10^{-4}	2.66 x 10^{-4}	1.09	2964.5	1.04	1.000
Activated carbon Layer: H_2	6.18 x 10^{-4}	1.24 x 10^{-3}	0.94	1171.0	8.53 x 10^{-4}	1.000
Zeolite Layer: CH_4	7.02 x 10^{-4}	1.40 x 10^{-3}	1.02	1795.9	5.34 x 10^{-4}	1795.9
Zeolite Layer: CO	6.45 x 10^{-4}	1.29 x 10^{-3}	0.87	2104.1	4.39 x 10^{-1}	429.43
Zeolite Layer: H_2	2.10 x 10^{-3}	4.21 x 10^{-3}	1.08	82.332	6.73 x 10^{-3}	796.29

Table C.3 - Parameters used for the Loading Ratio Correlation 3 isotherm, according to Yang et al. (1997) for case study 2

	IP1 (kmol/kg)	IP2 (1/bar)	IP3 (-)	IP4 (K)	IP5 (1/bar)	IP6 (K)
H_2	9.49×10^{-4}	1.89×10^{-3}	1.20	583.76	5.78×10^{-2}	149.82
CH_4	7.43×10^{-4}	1.49×10^{-3}	1.02	1795.9	5.34×10^{-4}	1795.9

Table C.4 – Calculated parameters for the Langmuir-Freundlich isotherm for case study 2

	IP1 (kmol/kg)	IP2 (kmol/kg/K)	IP3 (1/bar)	IP4 (K)	IP5 (-)	IP6 (K)
H_2	4.31×10^{-3}	-1.06×10^{-5}	2.52×10^{-3}	45.200	0.986	43.03
CH_4	4.89×10^{-3}	-8.96×10^{-6}	5.34×10^{-4}	1795.9	0.396	187.4

Appendix D – Bed Specifications for cases simulated in Chapter 5

Table D.1 – Specifications of the bed for the case study 1 (Section 5.1)

	Activated Carbon	Zeolite 5A
Layer length, H (m)	0.5	0.5
Internal bed diameter, d_{bi} (m)	3.71×10^{-2}	3.71×10^{-2}
Wall thickness, w_t (m)	1.34×10^{-3}	1.34×10^{-3}
Particle radius, r_p (m)	1.15×10^{-3}	1.57×10^{-3}
Bed packing density, ρ_b (kg/m^3)	482	746
Particle density, ρ_p (kg/m^3)	850	1160
Interparticle or bed porosity, ε_b	0.43	0.36
Intraparticle porosity, ε_p	0.61	0.65

Table D.2 – Specifications of the bed for the case study 2 (Section 5.2)

	Zeolite 5A
Layer length, H (m)	1
Internal bed diameter, d_{bi} (m)	4.40×10^{-2}
Wall thickness, w_t (m)	1.34×10^{-3}
Particle radius, r_p (m)	1.57×10^{-3}
Bed packing density, ρ_b (kg/m^3)	795
Particle density, ρ_p (kg/m^3)	1160
Interparticle or bed porosity, ε_b	0.315
Intraparticle porosity, ε_p	0.65

Appendix E - Attempts to use a constant feed flowrate during a PSA experiment

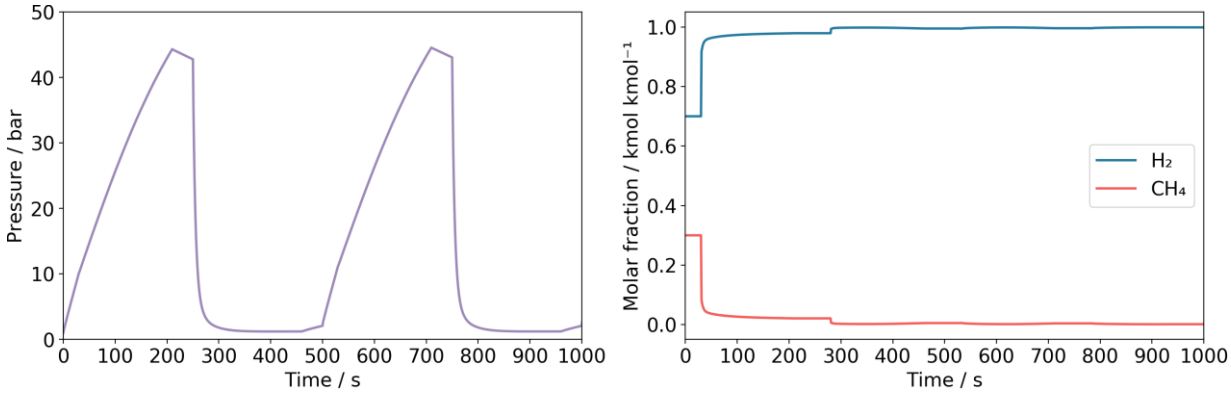


Figure E.1 - Results of a simulation run with a constant feed flowrate of 2.2 x 10^{-5} kmol/s during the whole cycle.

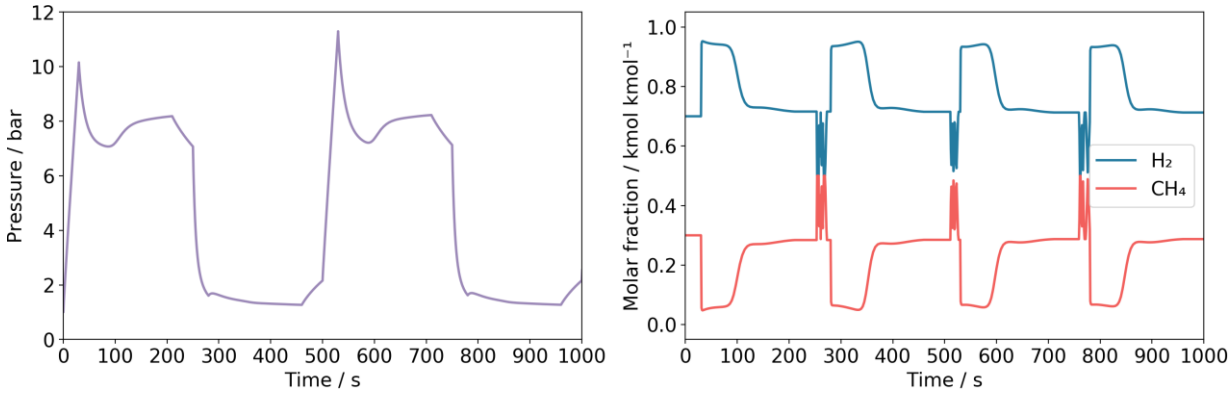


Figure E.2 - Results of a simulation run with a constant feed flowrate of 2.2 x 10^{-5} kmol/s during the whole cycle, increasing the purge and product valve's CV.

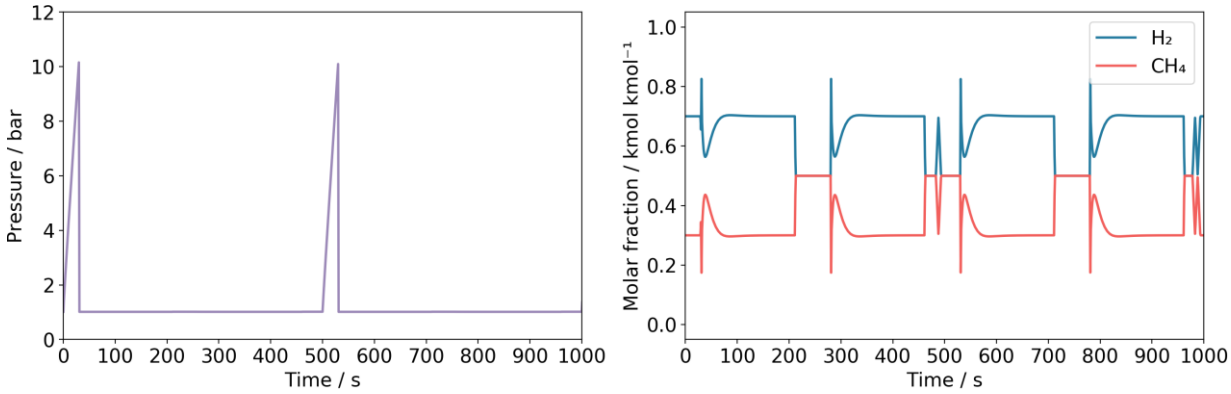


Figure E.3 - Results of a simulation run with a constant feed flowrate of 2.2 x 10^{-5} kmol/s during the whole cycle, leaving the purge and product valves completely open, so that the software calculates its flowrate.

Appendix F - Derivation of the CV expression for pressurization and depressurization valves

The derivation of the expression used to estimate the linear valve constant CV from the bed conditions and step time starts with the ideal gas equation:

$$P_B V_B = nRT_B \tag{F.1}$$

Where, P_B is the bed pressure, V_B is the effective volume of the bed, n is the number of moles in the bed, R is the ideal gas constant and T_B is the temperature of the bed.

The rate of change of pressure is related to the rate of change of material holdup, assuming constant temperature and volume:

$$\frac{\partial P_B}{\partial n} = \frac{RT_B}{V_B} \tag{F.2}$$

Since the flowrate through a valve can be expressed as a linear function of the pressure drop across the valve, and the flowrate can be expressed in terms of molar flux:

$$\frac{\partial n}{\partial t} = CV\ (P_B - P_{ext}) \tag{F.3}$$

Where the CV is the valve coefficient and P_{ext} is the pressure downstream the valve.

Assuming a constant downstream pressure from the valve, the rate of change of the pressure in the bed can be calculated from the following equation:

$$\frac{\partial P_B}{\partial t} = \frac{\partial P_B}{\partial n}\frac{\partial n}{\partial t} = \frac{RT_B}{V_B} CV\ (P_B - P_{ext}) \tag{F.4}$$

This expression can be integrated between the bed's start and end pressure for a given step duration and a constant external pressure:

$$\frac{RT_B}{V_B} CV\ dt = \int_{P_{Bstart}}^{P_{Bend}} \frac{1}{P_B - P_{ext}} dP_B \tag{F.5}$$

Giving,

$$CV = \frac{V_B}{R\,T_B t_{step}} \ln\left(\frac{P_{B\,start} - P_{Ext}}{P_{B\,end} - P_{Ext}}\right) \tag{F.6}$$